ResearchGate

See discussions, stats, and author profiles for this publication at: https://www.researchgate.net/publication/308802877

Phase transitions in ternary layered A 3 B 3 C 2 6 group ferroelectric semiconductors—A Review

Article *in* Turkish Journal of Physics · January 1994

CITATIONS
3

READS
73

4 authors, including:



Kerim Allakhverdiev
Milli Aviasiya Akademiyasi
178 PUBLICATIONS **2,458** CITATIONS
SEE PROFILE



Bulent Gultekin Akinoglu
Middle East Technical University
93 PUBLICATIONS **1,069** CITATIONS
SEE PROFILE



Şinasi Ellialtıoğlu
TED Universitesi
87 PUBLICATIONS **1,152** CITATIONS
SEE PROFILE

Some of the authors of this publication are also working on these related projects:

Analyzing Probable “Heat Island” Effect due to Large Scale Solar Power Plants in Turkey View project

Linking satellite imagery to bright sunshine hours for the estimation of global solar irradiation” (Küresel Güneş Işınımı Tahmin Etmek için Uydu Görüntülerini ve Güneşlenme Süresini Birleştirme) View project

All content following this page was uploaded by Şinasi Ellialtıoğlu on 30 October 2016.

The user has requested enhancement of the downloaded file.

THE SCIENTIFIC AND TECHNICAL RESEARCH COUNCIL OF TURKEY
TÜBİTAK
•1963•

TURKISH JOURNAL OF PHYSICS

volume 18 number 1 1994

Published by the Scientific and Technical Research Council of Turkey

Tr. J. of Physics
18 (1994) , 1 – 66.
© TÜBİTAK

Phase Transitions in Ternary Layered $A^3B^3C_2^6$ Group Ferroelectric Semiconductors A Review

K.R. ALLAKHVERDIEV[1,2], T.G. MAMEDOV[2], B.G. AKINOĞLU[1] and Ş.S. ELLİALTIOĞLU[1]

[1] *Middle East Technical University, Department of Physics, Ankara 06531–TURKEY*

[2] *Academy of Sciences of the Azerbaijan Republic, Institute of Physics, Azizbekov str. 33, Baku 370143–AZERBAIJAN*

Received 25.8.1993

Abstract

The physical properties of $A^3B^3C_2^6$ compounds in the range 6–300 K are discussed in the present review including the Brillouin scattering studies of dielectric properties and absorption spectra near the fundemental band gap. No attention has been given to the crystal luminescence below 4.2 K and to the physical properties of the ternary layered solid solutions.

1. Introduction

$A^3B^3C_2^6$ compounds are formed in the layered-chain structure as A^3C^6–B^3C^6 in which the components A^3C^6 and B^3C^6 have the ratio 1:1. For instance, in the compounds $TlGaS_2$, $TlGaSe_2$ and $TlInS_2$, the components are arranged in the form GaS–TlS, GaSe–TlSe, and InS–TlS, respectively, and they are called the "Ternary Layered $TlGaS_2$-type Chalcogenides".

Layered or as they are alternatively called quasi-two-dimensional compounds are characterized by high crystal structure anisotropy which enables us to consider their physical properties from a unified point of view. Even though the layered compound crystal structure contains a collection of alternating layers as in graphite, the number of layers within their unit cell can be more than one. Another peculiarity of the layered compounds is the easy cleavage into the plane-parallel mirror-like surfaces, so that samples which are convenient for surface property investigations can be produced.

Great interest to the study of the layered crystals is due to the fact that they have attractive unusual physical properties and exciting technical applications which can not be attained using non-layered anisotropic crystals. Typical examples are the followings :
– electron and phonon band splitting into the components which are equal to the number of layers in a unit cell;
– structural phase transitions (PT) followed by charge-density wave formation;
– existence of the low-frequency (rigid) interlayer modes in the optical phonon spectrum when the layers vibrate as an integral unity with respect to each other;
– possibility to find high-temperature superconductivity as anticipated by V.L. Ginzburg;
– possibility of intercalation of various atoms (molecules) between layers, and subsequent search of the effects on the weak interlayer interactions and other physical properties; etc.

Memory switching elements, emission modulators, nonlinear optical transducers and other semiconductor devices of quantum and optical electronics have been developed using layered compounds.

Different polytypes of the layered compounds exist and the main reason of the polytypism is the weak Van der Waals interactions between the layers. Hence, it may be possible to determine the polytypes using infrared (IR) and Raman scattering (RS) spectroscopies.

Discovery of low-temperature phase transitions (1977, [1]) and phase transitions under hydrostatic pressure (1979, [2]) in $A^3B^3C_2^6$ crystals enhanced the interest in their physical properties. Discovery of their ferroelectricity (1984, [3]) put them in a novel class of ferroelectrics. Of particular interest is the occurrence of incommensurate phase during the transition to the ferrophase.

The above topics and the works on vibrational excitation spectroscopy including the Brillouin scattering studies of dielectric properties and absorption spectra near the fundemental band in the range 6–300 K are discussed in the present review, but no attention is given to the crystal luminescence below 4.2 K and to the physical properties of the ternary layered solid solutions. All these discussions mainly cover the works performed at the Laser Spectroscopy Laboratory of the "Institute of Physics-Academy of Sciences of the Azerbaijan Republic".

2. Low Temperature Phase Transitions

The $A^3B^3C_2^6$ compounds were first synthesized by G. Offergeld [4] in 1963, and independently they were also grown by G. Guseinov [5] in 1967.

In the first 10–15 years, the reports mainly discussed the physicochemical [6–14] and physical [15–33] properties. Although the existence and some of the physical properties were unambiguously verified, their crystal symmetry was so far unresolved. Table 1 lists the structural data for $A^3B^3C_2^6$ compounds and the corresponding references[7–10, 34–42]. Except Ref.[36], clear and definite spatial arrangement of the atoms was not given in the literature. According to Ref.[36], the structure of the $A^3B^3C_2^6$ compounds could be represented by a two-dimensional alternate layers, each subsequent one rotated at right

angle to the preceeding one, and the probable space groups were C_s^4 or C_{2h}^6.

Table 1. Lattice Parameters and Crystal Structures for the $A^3B^3C_2^6$ Compounds

Compound	Structure	Symmetry	Parameters (Å)	z	Ref.
$TlGaSe_2$	TlSe	tetragonal	a=8.147;c=7.082	4	[34]
	"	"	a=7.626; c=30.56	16	[34]
	"	"	a=7.64; c=30.83	16	[7]
	"	"	a=7.644; c=30.832	16	[10]
	?	monoclinic	a=b=7.6		
			c=31–36, α=90.55^0	16	[35]
	$TlGaSe_2$	monoclinic	a=b=10.77		
			c=15.64, α=100.6^0	16	[36]
high-press. phase	TlSe	tetragonal	a=8.053; c=6.417	4	[37]
$TlGaS_2$	TlSe	tetragonal	a=8.075; c=7.06	4	[9]
	?	"	a=7.26; c=29.776	16	[7]
	"	"	a=7.295; c=29.70	16	[34]
	"	monoclinic	a=b=7.26		
		$P2_1/m$	c=4 × 19.4; α=90.20^0	32	[38]
	"	monoclinic	a=b=7.59		
		$P2_1$ or $P2_1/m$	c=59.99; α=90.17^0	32	[39]
	$TlGaSe_2$	monoclinic	a=b=10.29		
			c=15.28; α=100.08^0	16	[40]
$TlInS_2$	TlSe	tetragonal	a=7.47; c=30.0	16	[34]
α–$TlInS_2$	"	"	a=8; c=6.072	4	[7]
β–$TlInS_2$	"	"	a=7.752; c=29.698	16	[8]
$TlInS_2$	$TlGaSe_2$	monoclinic	a=b=10.95		
			c=15–14; α=100^0	16	[41]
low-temp.	?	rhombic	a=6.56; b=3.81		
modification		D_2^5	c=14.94	4	[41]
$TlInS_2$	?	triclinic	a=7.70; b=7.77		
		P_1	c=122; α=90.18^0		
			β=90.43^0; γ=90.10^0	64	[42]

Figure 1 shows the spatial pattern of $TlGaSe_2$ unit cell. Interpretation of vibrational spectra in $TlGaSe_2$ was inconsistent with C_s^4 space group [36]. Polarization analysis of long-wavelength IR and RS active phonon spectra in $TlGaSe_2$ has been interpreted on the basis of C_{2h}^6 space group [43]. The results obtained in Refs.[2, 43–46] also showed that the space group of $TlGaSe_2$ was C_{2h}^6. For C_s^4 space group [36], there was another disagreement because of the absence of second-harmonic generating signal in $TlGaSe_2$ excited by the 1.06 μm line of YAG:Nd^{3+} laser at room temperature. This disagreement might be due to the fact that in Ref.[36] a high temperature sublimate of $TlGaSe_2$ microcrystal has been studied, whereas in Refs.[2, 43–46], spectral studies have been performed on the Bridgman grown crystals. It is highly probable that $TlGaSe_2$ exhibits the polytypism which is characteristics of almost all the layered compounds.

The authors of Refs.[1, 47–48] were the first to pay attention to the anomalies at low-temperature IR and RS spectra of $TlGaSe_2$. Using the temperature dependence of IR and RS spectra, the anomalies were attributed to the probable existence of low-temperature phase transitions. In Ref.[49], the authors concluded that these transitions occurred on the surface of the crystals.

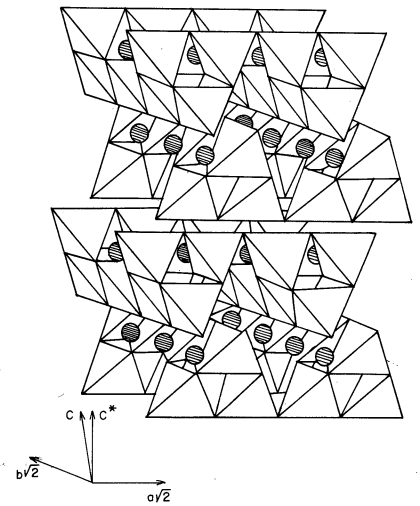


Figure 1. Spatial pattern of $TlGaSe_2$ unit cell [36]

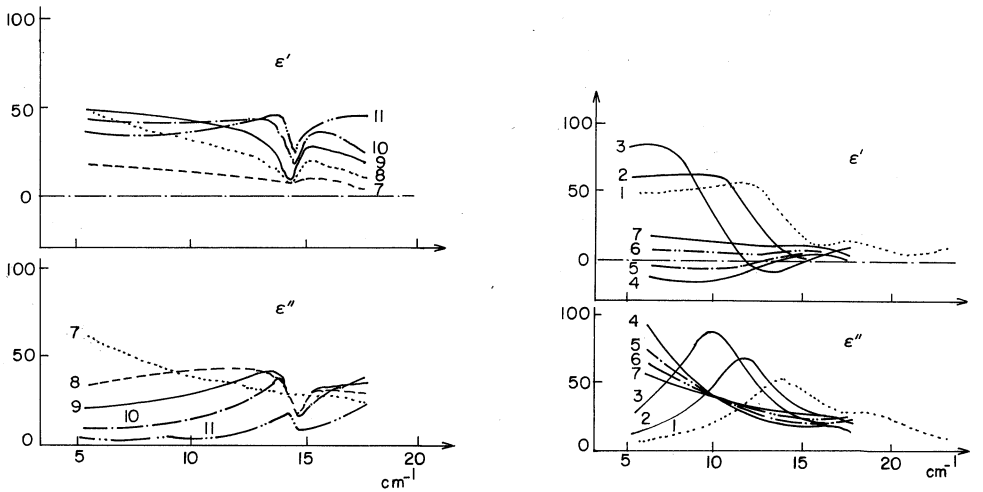


Figure 2. $TlGaSe_2$ submillimeter dielectric spectra at various temperatures. Curves 1-11 are for the temperatures 298, 244, 201, 123, 118, 113, 108, 106, 100, 94, 78 K, respectively

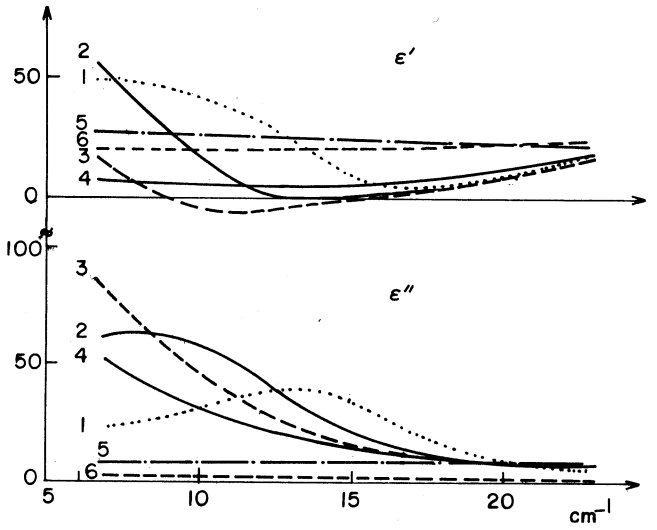


Figure 3. $TlInS_2$ submillimeter dielectric spectra at various temperatures. Curves 1-6 are for the temperatures 370, 294, 251, 206, 160, 86 K, respectively

Temperature-unstable polar vibrations with the soft optical mode features were detected in $TlGaSe_2$ [50] and $TlInS_2$ [51] by the submillimeter spectrometer developed at the Institute of General Physics of the Russian Academy of Sciences. In these works a possibility of ferroelectric state transitions was expected in the crystals. Figures 2 and 3 show the submillimeter dielectric spectra of $TlGaSe_2$ and $TlInS_2$, respectively, for different temperatures. Almost all the essential features for the permittivity coming from the real ($\epsilon'(\nu,T)$) and imaginary ($\epsilon''(\nu,T)$) parts of the dielectric function are rather similar for both crystals. These features can be summarized as:

a) temperature-unstable polar vibrations having soft mode features exist at $\nu \leq 20\ cm^{-1}$ ($\sim 14\ cm^{-1}$ in $TlGaSe_2$; $\sim 10\ cm^{-1}$ in $TlInS_2$). Vibration frequencies decrease as the temperature is lowered, whereas the dielectric contribution to the permittivity increases (curves 1–4 of Figure 2 and curves 1–3 of Figure 3);

b) the temperature ranges 120–107 K and 213–189 K for $TlGaSe_2$ and $TlInS_2$, respectively, are the intervals at which the dielectric dispersion changes its nature from resonance to relaxational one. The effect is vividly displayed in $\epsilon'(\nu,T)$ spectra at 7–10 cm^{-1} frequency range for $TlGaSe_2$ and $TlInS_2$ crystals, where ϵ' and its derivatives change their signs with frequency variations (curves 4–7 of Figure 2 and curves 4–6 of Figure 3);

c) at 107 K, dynamical properties of $TlGaSe_2$ alter drastically (curves 7 and 8 of Figure 2). A new strong absorption band reveals at 14 cm^{-1}, while soft mode shifts from the microwave region to the 15–20 cm^{-1} and loses its strength;

d) an unstable absorption mode appears below $\sim$ 9 cm^{-1} (curve 1 of Figure 3) in the absorption spectra of $TlInS_2$. Furthermore, the frequency independent behavior of ϵ'' is very typical for $TlInS_2$ at low temperatures (curves 5 and 6 of Fig.3).

To explain the temperature behavior of the soft mode parameters, $\epsilon'(\nu)$ and $\epsilon''(\nu)$ spectra were calculated by the least-squares technique, using one-oscillator dispersion model at each temperature point as the first approximation. Results of these calculations are presented in Figure 4. Natural frequencies are found to decrease critically with the temperature whereas ν_0^2 is linearly proportional to the temperature. The mode gives large dielectric contribution to the static permittivity whose values varies with temperature obeying Currie-Weiss law with constants C=5.5 $\times 10^3$ K and 5.3 $\times 10^3$ K for $TlGaSe_2$ and $TlInS_2$, respectively. Extrapolation of $\nu^2(T)$ to zero frequency at $T_1 = 107 \pm 2$ K point for $TlGaSe_2$ and $T_2 \simeq 189 \pm 2$ K point for $TlInS_2$ coincides with the jumpwise change in the temperature dependence of the dielectric function. Therefore, one could assume that the compounds had ferroelectric phase transitions at those temperatures and that the spontaneous polarization should occur below these temperatures [50–51].

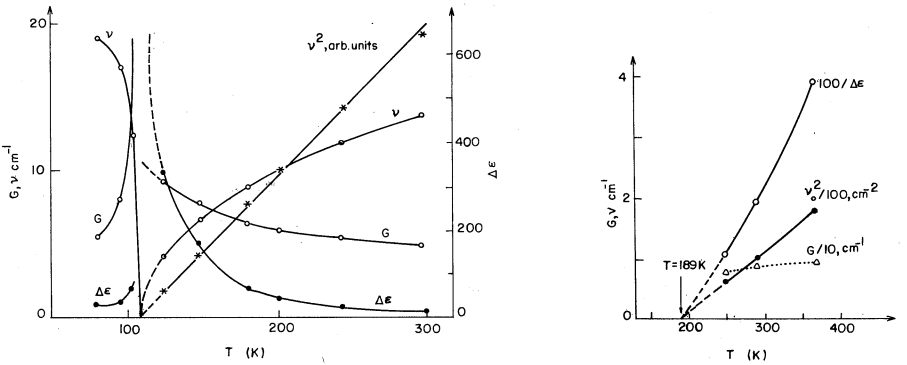


Figure 4. Soft mode parameters: $\nu, G, \Delta\epsilon$ as frequency, damping and dielectric contribution of $TlGaSe_2$ (top) and $TlInS_2$ (bottom)

When $\epsilon'(T)$ and $\epsilon''(T)$ curves were recorded in $TlGaSe_2$, a temperature hysteresis $\Delta T \sim 0.5$ K was observed at 107 K which was the evidence of the probable transition [50]. A dramatic change in soft mode frequency below 107 K also enhanced the possibility of such a phenomenon.

Dispersion changes from resonance to relaxational one at the temperature ranges 120–107 K and 213–189 K for $TlGaSe_2$ and $TlInS_2$, respectively, suggested that not a simple transition from para– to ferrophase occurs at 107 and 189 K. Presence of relaxational dependences of dielectric function on the temperature was known to be typical for the incommensurate phase transitions. For instance, similar behavior was observed in thiourea $SC(NH_2)_2$ [52]. Hence, by anology we could assume that the transformation to ferrophase in $TlGaSe_2$ (107 K) and in $TlInS_2$ (189 K) was preceded by long-periodic structure modulation waves in the crystals. Within the framework of this interpretation

relaxational nature of this dispersion at 107 K < T < 120 K ($TlGaSe_2$) and 189 K < T < 213 K ($TlInS_2$) could be attributed to the phase fluctuations of the ordering parameter which might have large dielectric contributions in such systems [52].

Further researches on the dielectric properties of $TlGaSe_2$ permitted to subdivide them into two groups. In the first group the data did not display any dielectric anisotropy when the incident wave polarization vector rotated in the cleavage plane and for such crystals the above mentioned temperature-frequency behavior was observed. In the second group, a dielectric anisotropy in the cleavage plane was found for $TlGaSe_2$ [53]. However, $TlInS_2$ crystals did not show any anisotropy in the dielectric spectra under the effect of rotation of the polarization vector.

Figure 5 shows the submillimeter spectra of the $\epsilon''(\nu)$ in one of the "abnormal" $TlGaSe_2$ specimens, recorded for the two orthogonal directions lying on the cleavage plane [53]. Here, the phase transitions soft mode can be clearly seen which is quite indistinguishable as shown by the authors of Ref.[50]. As the temperature decreased the spectra split into two parts for the two orthogonal directions of the polarization vector of the incident light, as shown in Fig.5. However, at room temperature, the dielectric properties of the crystal were in fact isotropic in the cleavage plane. The analysis showed that in one of the orientations, soft mode behavior was similar to that occurred in conventional "isotropic" specimens [50].

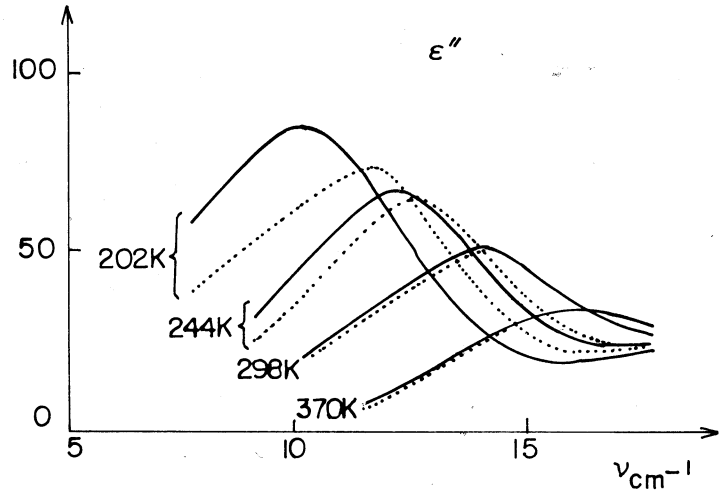


Figure 5. $\epsilon''(\nu)$ spectra of "abnormal" $TlGaSe_2$ for two mutually orthogonal orientations in the cleavage plane. Solid curves: soft mode with normal temperature bahavior [50]; dotted curves: soft mode splitting into two components upon temperature decrease (see Figure 6)

In one of the two orthogonal orientations, soft mode evolution upon specimen cooling developed in a different manner (Figure 6). As the temperature decreased, soft mode was broadened, and then split into two components of about the same intensity (curve 2 of Figure 6). The low frequency branch is almost identical to the normal crystal

mode except that the dielectric contribution is twice lesser.

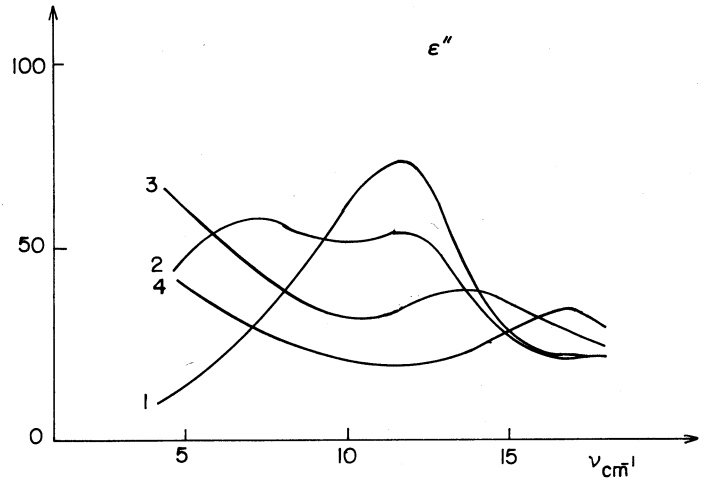


Figure 6. Low temperature $\epsilon''(\nu)$ spectra of "abnormal" $TlGaSe_2$ in one of the two orthogonal orientations. Soft mode component with abnormal temperature behavior is shown by arrows. Curves 1–4 are for the temperatures 202, 157, 138, 121 K, respectively

The second high frequency branch had a temperature-abnormal behavior. Its frequency varied with temperature monotonously. For this component the frequency was increased as the temperature approached to the T_1 and T_2 phase transition regions (Fig.7).

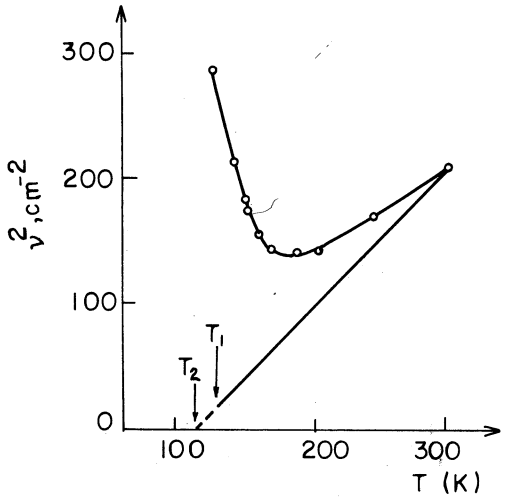


Figure 7. Temperature dependence of the frequency of two soft mode components in "abnormal" $TlGaSe_2$

In Ref.[53], all these different behaviors were attributed to the occurence of inetrlayer disordering [46] and to the various polytype formations of the layered ternary chalcogenides [54]. Due to the changes in the interlayer ordering for most of the specimens of these compounds, the crystal symmetries were increased from, say, C_{2h} to C_{4h} [46] and as a result dielectric isotropy was reached in the cleavage plane. The anisotropy reported in Ref.[53] was typical for the low-temperature measurements.

In Ref.[53], non-standard behavior of the soft mode temperature variation in $TlGaSe_2$ was explained by its interaction with another vibration. However, this interaction differed from the familiar mode relay transfer from one vibration to another. $TlGaSe_2$ is a long-wave modulation system so that some additional couplings between lattice modes may complicate the mode relay transfer [55]. In particular, the vibrations with different wave vectors $\mathbf{k}_1$ and $\mathbf{k}_2$ may couple when $\mathbf{k}_1$–$\mathbf{k}_2 = m\mathbf{q}$ where, $\mathbf{q}$ is the lattice modulation wavevector and m is an integer. Consequently, one of the modes can gain energy and increases its frequency while the other looses its energy when the mode vibration frequency is reached. In Ref.[56], however, submillimeter spectral features in abnormal $TlGaSe_2$ crystals were explained by a particular antiferromagnetic ordering in band electrons which results in non-zero toric moment. Transformation into toroidality was associated with a particular mode softening of the collective electron vibrations in the crystal [57]. In Ref.[56], it was shown that due to a specific nature of interactions between the toric moment and the electromagnetic field [58], behavior of the absorption coefficient near toric transition point differed dramatically, similar to the soft phonon mode dependence of the light scattering in the case of structural phase transition. Moreover, the frequency dependence of the absorption coefficient changes drastically in a magnetic field near toric transition, thus enabling us to separate the contribution of toric vibration.

In Ref.[56], it was shown that the temperature decrease results in a downshift in the toric absorption peak followed by a backward motion at a certain frequency. It was this behavior that was observed in the above mentioned "abnormal" $TlGaSe_2$ crystals [53]. Certainly, to confirm the existence of toric mode in $TlGaSe_2$ crystals, further experimental investigations on submillimeter absorption spectra at low temperatures and in magnetic fields of about 100 KOe are required. According to Ref.[56], when light-to-field orientation was $\mathbf{E} \perp \mathbf{H}$, the peak of the toric vibration downshifted as the field was increased and vanished at a certain value of the magnetic field. No such experiments have been carried out on $TlGaSe_2$ crystals, so far.

Appearance of Refs.[48–56] in the literature significantly increased the interest in the phase transition nature of $TlInS_2$ and $TlGaSe_2$ crystals, especially search on their ferroelectricity, dielectric spectroscopy studies of soft modes in solid solutios, structural studies of incommensurate phases, investigation of low-temperature IR and RS high-resolution spectra.

Soft optical modes in the vibrational spectra of $TlGa(S_{1-x}Se_x)_2$ mixed crystals were studied in Ref.[59]. No dielectric anisotropy was found in the cleavage plane for any of the composition. In contrast to the three absorption bands of $TlGaSe_2$ at $\nu_1 \sim 14\ cm^{-1}$, $\nu_2 \sim 19\ cm^{-1}$ and $\nu_3 \sim 32\ cm^{-1}$, submillimeter spectrum of $TlGaS_2$ had only one band

at $\nu_2 \sim 26\ cm^{-1}$. However, when the temperature of $TlGaS_2$ crystal was decreased to 170 K, another low-frequency band at 18 cm^{-1} was emerged in the spectra.

Fig.8a gives the temperature dependence of low-frequency soft mode ($\nu_1 \sim 14\ cm^{-1}$ for the solid solutions of $TlGa(S_{1-x}Se_x)_2$. The temperature coefficients A, that is the slope of the linear variation of ν_1^2 with the temperature are approximately the same for all compositions ($A = 1.1\ cm^{-1}$). For all the different compositions, soft mode tends towards zero frequency as the temperature is decreased but zero frequency is only achievable for low values of x (Figure 8a). Figure 8b shows the variation of the frequencies ν_1 and ν_2 with the concentration, at 100 K. The slopes of the curves considerably change at the composition $x = 0.7$ and at these concentrations most noticeable rearrangement in the mode intensities took place.

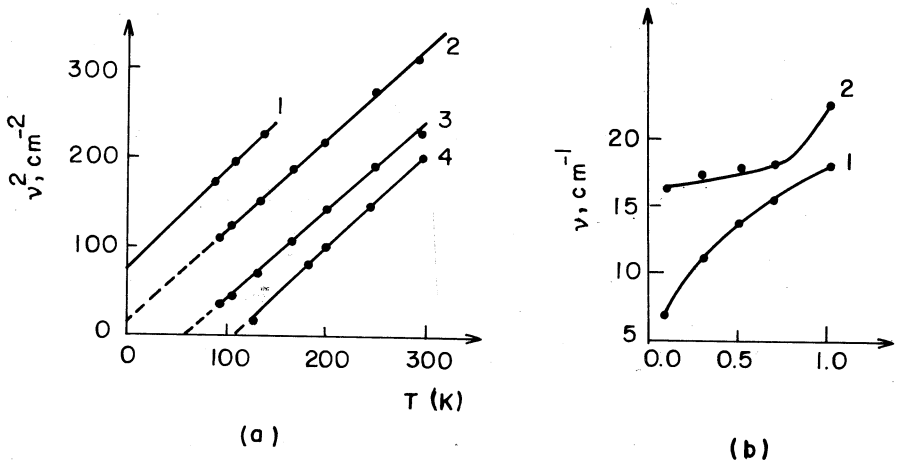


Figure 8. (a) Temperature dependence of the soft mode in $TlGa(Se_{1-x}S_x)_2$ for x values (1) 0.5, (2) 0.3, (3) 0.1, (4) 0. (b) Concentration dependencies of $\nu_1(1)$ and $\nu_2(2)$ for $TlGaS_2$ and $TlGaSe_2$ at 100 K

In addition to the solid solution studies, the investigations of the temperature dependence of static permittivity, spontaneous polarization and birefringence have also been carried out for $TlInS_2$, $TlGaSe_2$ and $TlGaS_2$ crystals [3]. Anomalies in the dielectric and optical spectra were recorded which indicated the presence of structural phase transitions in $TlGaSe_2$ at $T_1 = 119$ K and $T_2 = 107$ K and in $TlInS_2$ at $T_1 = 216$ K. A ferroelectric phase transition with spontaneous polarization value of $\sim 0.2\mu C/cm^2$ was found in $TlInS_2$ at 204 K. In the study of optical constants of the crystals, a special attention should be given to the orientation of the specimen. For the specimen surface the layer of which was peeled along cleavage plane, conoscopic patterns shift from the center, i.e., optical indicatrix is turned through an angle ϕ_o of approximately 2° about the cleavage plane axis as seen in Fig.9. Therefore, $TlGaSe_2$ and $TlInS_2$ are monoclinic. $TlGaS_2$ has a pattern typical for uniaxial crystals. In Figure 9, z' is a pseudotetragonal axis

perpendicular to the principle cleavage plane ($TlGaSe_2$ has, besides, two complementary planes of less perfect cleavage lying 45° to the x' and y'). The optical indicatrix y axis coincides with the C_2 crystallographic axis (or is perpendicular to the cleavage plane). The axes z and z' are misdirected by a small angle ϕ, same as the x and x' axes and z axis bisects the acute angle between the optical axes. For $TlGaSe_2$ $n_z = n_g$, $n_y = n_p$, $n_x = n_m$ and for $TlInS_2$ $n_z = n_g$, $n_y = n_m$, $n_x = n_p$. Therefore, z-cut gives negative birefringence, $n = n_y - n_x$, for $TlGaSe_2$ and positive for $TlInS_2$. Conoscopic pattern studies through the polarizing microscope show monoclinic symmetry to be retained over the range 80–560 K. In particular, no symmetry reduction to triclinic and no ferroelectric domains were found under low-temperature phase transitions. Presence of uniaxial points should be mentioned in $TlGaSe_2$ at 115.5 K and in $TlInS_2$ near 480 K. No transition to the tetragonal phase was observed up to 560 K [3] (which might be expected from the pseudosymmetric nature of the phase at room temperature).

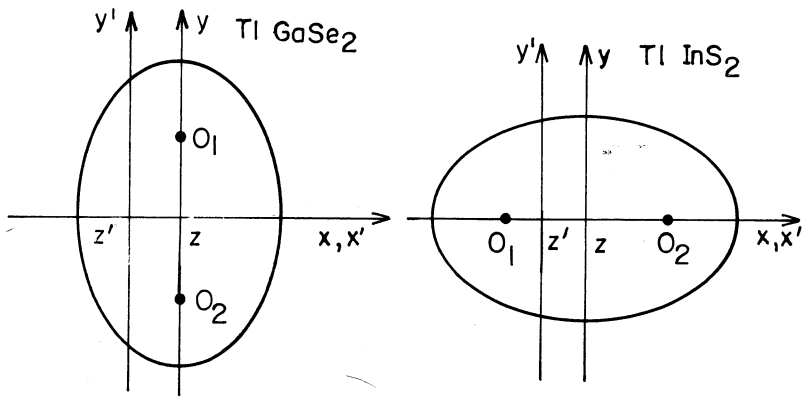


Figure 9. Coordinate axis (x', y', z') of a wafer and (x, y, z) of optical indicatrix. O_1 and O_2 are optical axes. First isochromatic oval is a fragment of conoscopic pattern observed for 1 μm-thick (001) cleavage plane-spalled wafers in a polarizing microscope. Thick line gives a monoclinic symmetry plane projection

Even though the crystals $TlGaSe_2$, $TlInS_2$ and $TlGaS_2$ posses monoclinic symmetry, no anisotropy of permittivity on the cleavage plane could be observed. Therefore, the real part entries ϵ'_x and ϵ'_y of the permittivity tensor were the same. According to Ref.[3], the values ϵ'_x were 37, 67 and 25 for $TlInS2$, $TlGaSe_2$ and $TlGaS_2$, respectively, while $\epsilon'_z \simeq 16$ for all, at $T = 300$ K.

Anomalies in ϵ'_x were observed at the temperatures $T_1 = 216$ K and $T_2 = 202$ K for $TlInS_2$ (Fig.10) which suggested the presence of a structural phase transition [3]. Similar anomalies were also found at $T_1 = 119$ K and $T_2 = 107$ K in $TlGaSe_2$ (Fig.11). In the temperature ranges $T - T_1 < 50^0$ and $4^0 < T_2 - T < 30^0$, the functions $\epsilon'_x(T)$ for $TlInS_2$ and $TlGaSe_2$ could be represented by Curie-Weiss law

$$\epsilon'_x = \frac{C}{(T - T_0)}, \tag{1}$$

where T_0 is the Curie-Weiss temperature. The Curie constant in the high temperature range (i.e., for $T - T_1 < 50^0$) was determined to be $C^+ = 5.3 \times 10^3$ and 5.4×10^3 K for $TlInS_2$ and $TlGaSe_2$, respectively, whereas in the low-temperature range they took the values $C^- = 1.4 \times 10^3$ and 1.6×10^3 K.

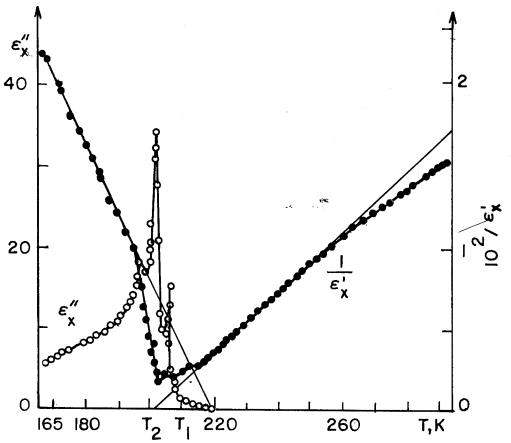


Figure 10. Temperature dependences of $(\epsilon'_x)^{-1}$ and ϵ''_x of $TlInS_2$ at 100 kHz

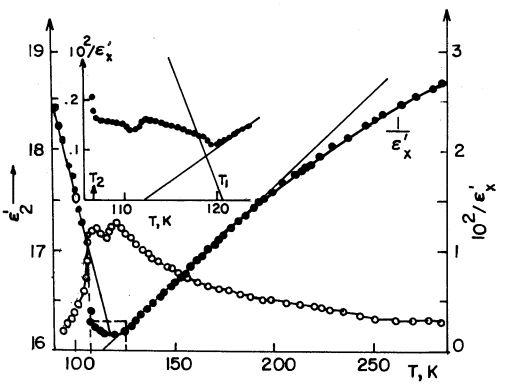


Figure 11. Temperature dependences of $(\epsilon'_z)^{-1}$ and ϵ'_z of $TlInS_2$ at 100 kHz

In both of the crystals $TlGaSe_2$ and $TlInS_2$, phase transitions at temperature T_1 were the first order. At $T = T_1$, ϵ'_x was finite which was non-standard compared to the usual ferroelectric transitions. For $TlInS_2$, phase transition at $T = T_2$ was second order, whereas in $TlGaSe_2$ the transition was again first order with a temperature hysteresis of $\leq 0.5^0$ [3].

As the temperature was increased a sharp increase was observed in the temperature variation of the imaginary part of the dielectric contribution to the permittivity (ϵ''_x), reaching a peak at $T = T_2$ (Fig.10). A number of extra peaks were also observed in the temperature range $T_2 < T < T_1$, which could be reproduced upon cooling and heating of the specimens.

At low temperatures ($T \leq T_2$), dielectric hysteresis loops were observed which indicated the ferroelectric nature of the $TlInS_2$ crystals. Below T_2, spontaneous polarization increased rapidly reaching a value of about 0.19 $\mu C/cm^{-2}$ at $T_2 - T \leq 40^0$. Cohercive field at these temperatures was around 350 V/cm [3].

Within the temperature range studied in Ref.[3], no dielectric hysteresis loop were found in $TlGaSe_2$ since the detection of such a loop for $T \leq T_2$ was complicated due to a considerable increase in the dielectric losses or the conductivity properties in strong electric fields (1–4 kV/cm). However, soon after the publication of Ref.[3], dielectric hysteresis loops were found in $TlGaSe_2$ by R. Bauchower (unpublished results) and by N.A. Bakhyshev (unpublished results).

Temperature variation of ϵ'_x and ϵ'_z showed no anomalies up to 90 K for $TlGaS_2$. ϵ'_x varied with the temperature as in Eqn (1), where $C = 3 \times 10^4$ K over the entire range studied.

Temperature dependence of the birefringence $\Delta n = n_y - n_x$ was obtained in Ref.[3] as plotted in Fig.12 for $TlInS_2$. As it can be seen from this figure, except a second-order phase transition at $T_1 = 216$ K, no other transition was observed in the temperature dependence of birefringence. The value of Δn just above T_1 is 1.1×10^{-4} and decreases with a rate of $d\Delta n/dT = -2.1 \times 10^{-7}$ K^{-1}. In $TlGaSe_2$, however, two transitions were found at $T_1 = 119.6$ K (second-order) and at $T_2 = 107$ K (first-order) having 1^0 hysteresis. At 120 K, $\Delta n = -0.9 \times 10^{-4}$ and is increasing with a rate of 0.73×10^{-7} K^{-1}.

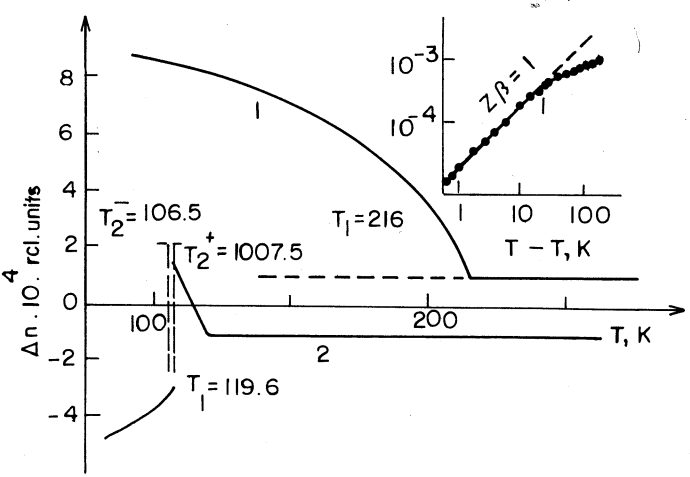


Figure 12. Temperature variation of the birefringence $\Delta n = n_y - n_x$ ($\lambda = 6328$ Å) for $TlInS_2$ (1) and $TlGaSe_2$ (2)

Large anomalies in the temperature variation of ϵ'_x for $TlInS_2$ and $TlGaSe_2$ agreed with the reduction of the optical soft mode frequency at **k**=0 observed in one of these crystals [50]. The value of the Curie constant 10^3 K was typical as encountered in

the order-disorder transitions where the homogeneous polarization serves as transition parameter. On the other hand at T_1, large deviation (10^0) between T_1 and T_0 indicated that the polarization could not serve as a transition parameter at $T = T_1$. Besides, the value of the spontaneous polarization was too small to explain large anomalies in the temperature dependence of the birefringence at the phase transition.

Two possible qualitative explanations of the observed anomalies in the temperature variation of the dielectric constant and in the birefringence were given in Ref.[3]. One of them was that the crystal $TlInS_2$ being a ferroelectric, where the polarization and antipolarization coexist, the former of which was around 1 $\mu C/cm^2$ and principally contributed to the variation in Δn. The second explanation was that the crystal was an improper ferroelectric, and its principal contribution to Δn was due to the interaction between the multi-component ordering parameter and the deformation. In this case, the crystal might transform into an incommensurate phase below T_1 and the second phase transition at 204 K should result in a homogeneous spontaneous polarization which was observed in the experiments. Δn in $TlInS_2$ do not contradict the possible transition into a commensurate phase at T_2. These transitions generally cause deformation and that is why Δn varies smoothly with the temperature.

Although, spontaneous polarization was not observed for $TlGaSe_2$, dielectric and optical anomalies were similar to $TlInS_2$, which suggested that their phases were identical in the range $T_2 < T < T_1$. At T_2, anomaly in the temperature variation of Δn was not typical for lock-in transitions from an incommensurate to a commensurate phase.

Alteration of dielectric dispersion nature from resonant to relaxational one [50, 51] and the low-temperature variation of the dielectric and optical properties at the transition points [3] increased the interest in the studies of the transition nature and searches for incommensurate phases in $TlInS_2$ and $TlGaSe_2$. Some measurements were performed using three-axis neutron spectrometer with 2.44 Å beam, for $TlInS_2$ in [60] together with dilatometric measurements. Figures 13 and 14 show the results of these measurements. Anomalies at 220 K, within the range 202–195 K, and at 170 K are clearly seen on $\alpha(T)$ curve [60].

Figure 14 shows the results of neutron scattering studies of $TlInS_2$. Shaded peaks correspond to principle reflections by a high-temperature monoclinic modification whereas the peaks with q_1=(0; 0; 0.25) are the reflections due to superstructural modification. This indicates the quadruplication of the unit cell. Several weaker peaks observed with $q_2 = \frac{1}{3}q_1$ and yet ambigious nature were also seen.

Two-dimensional distribution of the scattering intensity studies in the (110) and $(1\bar{1}0)$ planes near $(\bar{1}; 1; 1.25)$ and (1; 1; 1.25) peaks showed that in the range 216–200 K an incommensurate phase in $TlInS_2$ crystal existed and it was characterized by $\mathbf{k}_i$=(δ; δ; 0.25) wave-vector where $\delta = 0.012 \pm 0.003$. A commensurate phase with q_1 and a new type of deviation from incommensurability with q_2 were found below 200 K (Fig.14). The value and direction of this deviation were not determined and they might be the peaks of another modification.

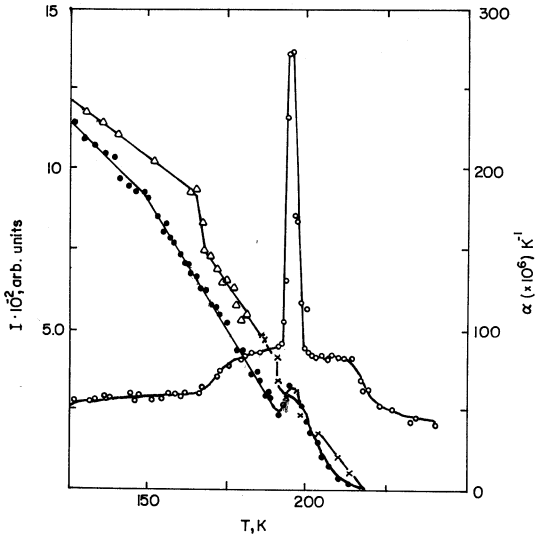


Figure 13. Temperature variation of the expansion coefficient (curve 1) and scattered neutron intensities at the point (1:1:1.25) (curves 2 and 3)

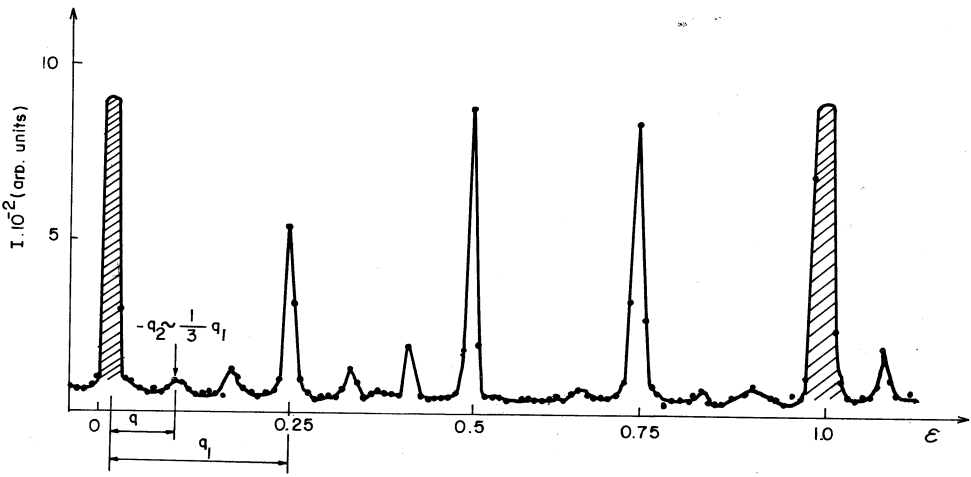


Figure 14. A section of neutron diffraction pattern for $TlInS_2$ at 80 K (scan is from (110) site towards [001] direction.)

Measurements of expansion coefficients of $TlInS_2$ single crystals in the directions parallel and perpendicular to the cleavage plane ($\alpha_\perp$ and $\alpha_\parallel$) revealed an interesting feature [61]. When the temperature was around 200 K a strong anomaly was detected in

$\alpha_\perp$. A sharp increase up to a value 2×10^{-4} K^{-1} was recorded which was the highest value observed in layered crystals. Weaker anomaly was observed in the temperature dependence of the expansion coefficient $\alpha_\perp$ near 170 K. The temperature dependence of $\alpha_\parallel$ was permanent over the range 40 to 200 K. This experimental observation suggested the same conclusion concerning the phase transition nature in $TlInS_2$ near 200 K.

Expansion coefficients for uniaxial crystal $TlInS_2$ with quasitetragonal structure approximation can be expressed as:

$$\alpha_\perp = \frac{C}{V}\left[\frac{C_{11}+C_{12}}{(C_{11}+C_{12})C_{33}-2C_{13}^2}\ \gamma_\perp - \frac{2C_{13}}{(C_{11}+C_{12})C_{33}-2C_{13}^2}\ \gamma_\parallel\right], \tag{2}$$

$$\alpha_\parallel = \frac{C}{V}\left[\frac{C_{33}}{(C_{11}+C_{12})C_{33}-2C_{13}^2}\ \gamma_\parallel - \frac{C_{13}}{(C_{11}+C_{12})C_{33}-2C_{13}^2}\ \gamma_\perp\right], \tag{3}$$

where C is specific heat, V is volume, C_{ik} are elastic coefficients and, $\gamma_\parallel$ and $\gamma_\perp$ are Grüneisen parameters.

Layer structure suggests that the elastic coefficients C_{13} and C_{33} describing interlayer forces are much lower than the elastic coefficients C_{11} and C_{12} describing the intralayer forces. Then, the linear expansion coefficients can approximately be written as:

$$\alpha_\perp \simeq \frac{C}{V}\frac{1}{C_{33}}\ \gamma_\perp, \tag{4}$$

$$\alpha_\parallel \simeq \frac{C}{V}\frac{1}{(C_{11}+C_{12})}\ \gamma_\parallel. \tag{5}$$

Near the transition temperatures, large anomalies were observed in $\alpha_\perp$ while $\alpha_\parallel$ remained almost constant [61] which suggested that a large decrease in C_{33} took place as a result of increasing in interlayer separation. However, intralayer interactions did not vary significantly under phase transition since the elastic coefficients C_{11} and C_{12} remained almost constant.

The variations of the expansion coefficients with the temperature for $TlInS_2$ and $TlGaSe_2$ were not similar. For example, for $TlGaSe_2$ [62], anomalies were also observed in $\alpha_\parallel(T)$ as shown in Fig.15. In this figure, three anomalies in $\alpha_\perp(T)$ can be seen at the temperatures $T_1 \simeq 120$ K, $T_2 \simeq 111$ K and $T_3 \simeq 102$ K where the first two are at the same points as in the dielectric anomalies [1, 50]. At around the same temperature that the third anomaly was observed, similar behavior was reported in the energy level analysis of exciton absorption band [63]. Unlike the crystal $TlGaSe_2$, $TlInS_2$ did not show sharp anomaly at the temperature $T_1 \sim 120$ K.

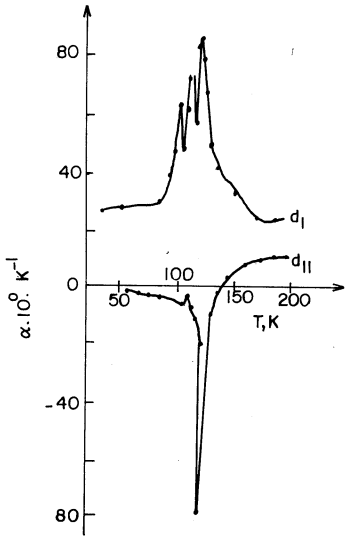


Figure 15. Temperature variation of linear expansion coefficient for $TlGaSe_2$ in two mutually perpendicular directions

Negative expansion coefficient was also observed in the crystals C, BN, GaS, GaSe, and InSe [64–67] and was attributed to the predominant contribution of transverse acoustic waves with displacement vector normal to the layers. However, such a mechanism suggested that, when the waves were propagating through the layer plane different dispersion relations existed for the polarization vector normal and parallel to the layers. Corresponding phonon dispersion curves for $TlGaSe_2$ [68], gave practically similar dispersion laws for the two types of acoustic vibrations mentioned above. The distinction between the dispersion relations of $TlGaSe_2$ and C, BN, GaSe is presumably related to a more complicated structure of the former crystal.

An alternative explanation of negative expansion coefficient region might be the compression of the layer as a result of a strong expansion towards weaker bonds. However, this description dos not explain the temperature behavior of $\alpha_{||}$ since both of the expansion coefficients have similar behavior at $T \simeq 120$ K.

It was assumed that the reasons for the appearence of the phase transition at 120 K were the structure modulation along the **c**-axis and layer deformation in the plane perpendicular to the **c**-axis [68]. The behavior of the expansion coefficient in $TlGaSe_2$ were similar to those theoretically anticipated [69] at $T_1 = 120$ K for the lock-in transitions.

Neutron diffraction measurements in $TlGaSe_2$ were reported in [68], which were carried out to refine the space group and to investigate incommensurate phases at low temperatures. Two types of diffraction patterns were obtained which led to a conclusion about the existence of at least two polymorphic modifications that would be later referred

to as $\alpha-$ and $\beta-TlGaSe_2$. Fig.16a gives a part of the neutron diffraction pattern for $\alpha-TlGaSe_2$ measured at room temperature (Diffraction pattern indexing is given in terms of basis vectors for a base-centered monoclinic structure primitive cell as: $\mathbf{a}_{p2} = (\frac{a_m}{\sqrt{2}}; \frac{b_m}{\sqrt{2}}; 0)$, $\mathbf{b}_{p2} = (\frac{a_m}{\sqrt{2}}; \frac{b_m}{\sqrt{2}}; 0)$, $\mathbf{c}_{p2} = (0; 0; c_m)$). The indices of the reflection peaks indicate that the structure is monoclinic.

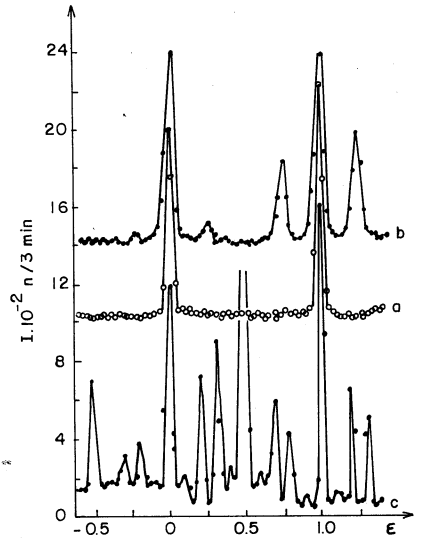


Figure 16. A section of $TlGaSe_2$ diffraction pattern from (300) site towards [001] : (a) α-modification at 300 K, (b) α–modification at 80 K, (c) β–modification at 300 K

Figure 16c shows similar diffraction pattern for $\beta-TlGaSe_2$ at room temperature. In this case, it can be observed that in addition to $(h, 0, k)$, normal monoclinic reflection peaks and some strong $(h, 0, k+0.5)$-type and weaker $(h, 0, k+\mathrm{m} \times 0.1)$-type reflection peaks are also present. Both types of these extra peaks were observed at $h = 2n+1$ and absent at $h = 2n$. The pattern in Fig.16c suggests that lattice modulation exists in $\beta-TlGaSe_2$ which results in the long periodic structure formation with modulation period $C_{mod} = 10c = 160$ Å (**c**-axis is perpendicular to the layers).

The most probable reasons of the formation of modulated structure in layered crystals are the existence of various stacking faults. In some works a pseudotetragonal diffraction pattern was observed in $TlGaSe_2$ so that one could assume that the structure modulation was due to the microtwin presence located at an angle of 90^o with respect to each other. A long periodic pseudotetragonal cell with a modulated **c**-axis (20c) period might be constructed from these microtwins. However, this description does not give the reasons of the absence of superstructural peaks at $h = 2n$.

All these contradictions could be overcome if one assumes that the observed structure modulation was due to the rotation of microtwins by 180^0 rather than 90^0. This assumption can only be valid if a pseudotetragonal symmetry can be found for some definite families of the reflection peaks. This fact is illustrated in Fig.17 where $TlGaSe_2$ primitive cell is shown before and after rotation ($\mathbf{a}_1$, $\mathbf{b}_1$, $\mathbf{c}_1$, and $\mathbf{a}_2$, $\mathbf{b}_2$, $\mathbf{c}_2$, vectors respectively, Fig.17a) together with appropriate reciprocal lattice vectors (Fig.17b). Fig.17c shows the formation of modulated structure by layer rotation through 180^0 in every 5 periods and the resulting unit cell is given by dotted line.

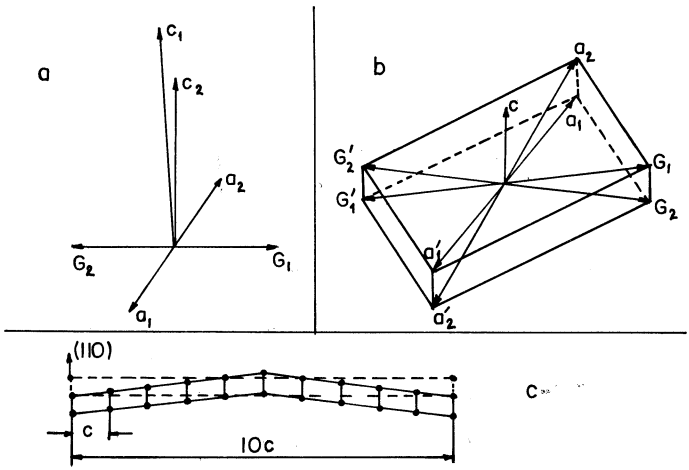


Figure 17. Long-periodic pseudotetragonal structure formation in β–$TlGaSe_2$

Structural factor calculations for such a modulated structure explain the absence of superstructural reflection peaks at h=2n observed in the experiments. The maxima in the neutron diffraction pattern of Fig.16 for $\beta-TlGaSe_2$ coincides the superstructural sites of the proposed model. But for a final confirmation, measurements using the four-circle neutron diffractometer must be carried out.

Neutron diffraction pattern analysis also demonstrates that a phase transition accompanied by unit cell quadruplication takes place in $\alpha-TlGaSe_2$ near 120 K. Fig.16b gives the neutron diffraction pattern for $\alpha-TlGaSe_2$ at 80 K in which the superstructural reflection peaks of $(h,\ 0,\ l+0.25)$-type can be clearly seen. These reflection peaks and the extra ones as well are absent in $\beta-$modification for even h. A study was undertaken to find out whether this transition is accompanied by an intermediate incommensurate phase, as in $TlInS_2$ [60]. However, deviations in the superstructural reflection peaks of the commensurate phase were observed. The result was in good agreement with the above proposed β-$TlGaSe_2$ structural model since coherent domain advancement of 5 unit cells along the **c**-axis already took place, the probability of another cell multiplication inside such a coherent domain is very small.

Transverse low-frequency phonon dispersions [68] in the directions [100] and [001] for $TlGaSe_2$ were studied (Fig.18). It was observed that the acoustic phonon frequencies in the direction perpendicular to the layers (i.e., [001] direction) were much lower than those in the intralayer direction [100]. Such behavior is typical for layered crystals and confirms the fact that intralyer interionic couplings are stronger than the interlayer ones. It is interesting to note that TlSe does not have this feature which reveals the fact that partial Tl substitution in place of Ga affects both bond structure and nature.

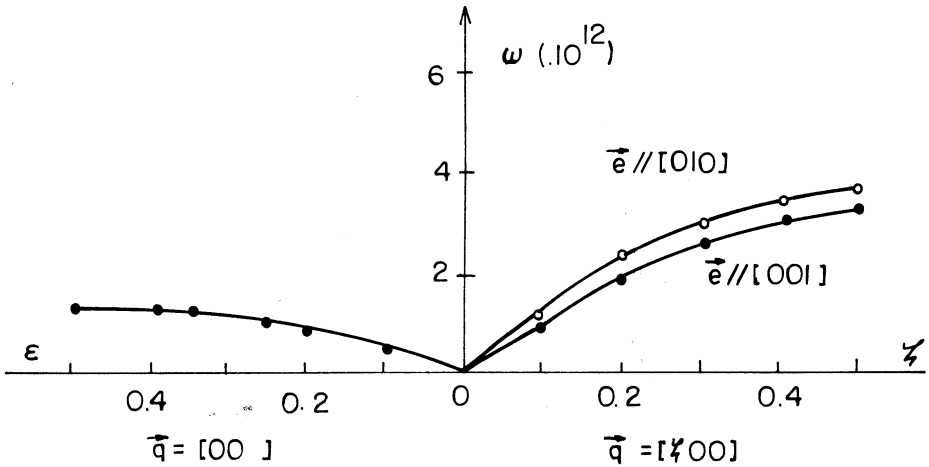


Figure 18. Dispersion curves of transversal low-frequency phonons for $TlGaSe_2$ in the directions [100] and [001]

Temperature behavior of the heat capacity and the components of the expansion coefficients for incommensurate phase of $TlInS_2$ and $TlGaSe_2$ in terms of thermodynamic theory were reported in Ref.[70]. Comparison of the theoretical and experimental results leds to the determination of appropriate thermodynamic potential parameters.

It becomes obvious that ternary layered chalcogenides show a series of low-temperature phase transitions followed by a ferroelectric one. Analyses of the dielectric and optical spectra, neutron diffraction and thermal measurements permit to conclude that the ferroelectric phase transition is preceded by incommensurate phase formation.

Besides all the above mentioned works, the experiments on the long wavelength IR [70–72] and RS [71–75] spectroscopy of $A^3B^3C_2^6$ crystals at their low temperature phase transition region was also performed. In these reports, vibrational spectra were assigned to different space groups of these crystals. Following discussions contain a brief presentation of the vibrational spectra of $A^3B^3C_2^6$ crystals on the basis of various space groups, since x-ray data are ambiguous as noted above.

According to Ref.[44], the crystals have C_c^2 symmetry group, and the unit cell contains 16 formula units (2 layers). In this approximation, decomposition of the vibrational representation into irreducable one for **k**=0 yields:

$$\Gamma = 23A_g + 25B_g + 23A_u + 25B_u \tag{6}$$

where $A_u + 2B_u$ and $A_g + 2B_g$ are acoustic and optical interlayer modes, respectively. Following the selection rules, one can obtain that $23\,A_g + 25B_g$ modes are RS active while $22\,A_u + 23B_u$ are IR active.

In Ref.[2], however, it was stated that the crystals have C_{2h}^6 symmetry group so at $\mathbf{k}$=0 vibrational representation is:

$$\Gamma = 10A_g + 14B_g + 10A_u + 14B_u \tag{7}$$

where $A_u + 2B_u$ are acoustic modes. $9\,A_u$ ($\mathbf{E} \parallel \mathbf{c}$) and $12\,B_u$ ($\mathbf{E} \perp \mathbf{c}$) IR active and $10\,A_g + 14B_g$ RS active modes should be expected.

Another representation was proposed in Ref.[46] with the assumption that the primitive cell contains 8 formula units, and at $\mathbf{k}$=0 it was given as:

$$\Gamma = 7A_{1g} + 3A_{2g} + 8B_{1g} + 2B_{2g} + 14E_g + 2A_{1u} + 8A_{2u} + 3B_{1u} + 7B_{2u} + 14E_u \tag{8}$$

where $7A_{1g} + 8B_{1g} + 2B_{2g} + 14E_g$ are RS active modes and $7A_{2u} + 13E_u$ are IR active ones.

The most comprehensive search on IR and RS spectra in $TlInS_2$ over 6–300 K and 5–400 cm^{-1} ranges was presented in Ref.[71]. Figures 19 and 20 show the reflection spectra at various temperatures for $TlInS_2$ in $\mathbf{E} \perp \mathbf{c}$ and $\mathbf{E} \parallel \mathbf{c}$ geometries, respectively. Table 2 lists LO and TO phonon frequencies at room temperature determined by Kramers-Kronig relation using the reflection spectra. Table 3 gives the frequencies of IR active phonos in $TlInS_2$ at 80 and 6 K. The transmission spectra for the geometry $\mathbf{E} \perp \mathbf{c}$, in the range 5–50 cm^{-1} shows absorption bands at 8.5, 12.0, 16.5, 19.2, 30.7 and 45.5 cm^{-1} for $TlInS_2$ [72]. Analysis of the data presented in Table 2 and 3 show that the authors of Ref.[71] discovered all 12 B_u-type and 5 A_u-type phonons anticipated by symmetry theory for C_{2h}^6 space group. Four A_u-type phonons could not be observed in Ref.[71] due to weak oscillator strengths and to the frequencies which were out of the range. The reason is that the production of thin slabs having several tens of μm thickness with a reflecting surface in the **c**-axis is almost impossible in the layered crystals.

No significant changes were found in the reflection spectra upon cooling of the crystal down to 260 K [71]. At this temperature, a weak shoulder appeared on the low- and high-frequency tails of the I and II bands, respectively. Some faint features were also observed at this temperature in the $\mathbf{E} \parallel \mathbf{c}$ spectra. Subsequent cooling demonstrated clearer spectra in both geometries (curves 2 in Figs.19 and 20).

According to Ref.[60], $TlInS_2$ has incommensurate phase with $q_{inc} = (\delta;\ \delta;\ 0.25)$ over the range 216–200 K. The IR measurements also showed that the largest spectral changes occured at this temperature range (curves 2 and 3 in Figures 19 and 20). Considerable changes occured for $\mathbf{E} \parallel \mathbf{c}$ geometry in the low-frequency region of the spectrum. A new band, IV″ appeared near the band IV′ (curve 3 in Fig.20) with LO–TO splitting at

102–98 cm^{-1}. Another new B_u-type band appeared also in $\mathbf{E} \perp \mathbf{c}$ geometry with LO–TO splitting at 171–173 cm^{-1} and 80 K (see Table 3). New spectral bands over the range 220–180 K (Figures 19 and 20) are presumably due to structure modulations accompanied by the commensurate phase with $q_1 = 0.25$ [60]. Subsequent cooling to 170 K resulted in the lock-in transition with quadruplication along the **c**-axis and a new type of departure from incommensurability develops within the same temperature range of 200–170 K [60].

Table 2. The IR active phonon frequencies in $TlInS_2$

$\mathbf{E} \perp \mathbf{c}$ polarization							$\mathbf{E} \parallel \mathbf{c}$ polarization						
	our work		[7]		[24]			our work		[7]		[24]	
band	TO	LO	TO	LO	TO	LO	band	TO	LO	TO	LO	TO	LO
yII	32	38	33	33	30	38	–	–	–	–	–	–	–
yI	49	55	48	54	–	–	–	–	–	–	–	–	–
y	89	99	89	97	80	96	y^I	66	78	65	77	66	77
Iy	132	145	129	142	124	144	Iy^I	114	118	114	117	112	116
III	271	284	265	278	264	282	III^I	162	176	166	175	160	176
II	304	334	297	329	295	332	II^I	282	304	280	300	280	300
I	348	350	–	–	–	–	I^I	332	350	325	345	328	348

Table 3. The IR active phonon frequencies in $TlInS_2$ at 80 and 6 K. Weak bands with small LO–TO splitting at 80 and 6 K are denoted as "weak" for both geometries.

$\mathbf{E} \perp \mathbf{c}$ polarization								$\mathbf{E} \parallel \mathbf{c}$ polarization							
80 K				6 K				80 K				6 K			
N	TO	LO	band	N	TO	LO	band	N	TO	LO	band	N	TO	LO	band
	36	42	VII		37	44	VII		70	77	V′		70	78	V′
	49	56	VI		51	58	VI		98	103	IV″		99	103	IV″
2	90	93	V	3	91	93	V					3	weak		
1	95	102	V	2	95	97	V					2	111	113	IV′
				1	98	102	V		115	118	IV′	1	115	118	IV′
3	132	133	IV	3	132	133	IV		163	175	III′		163	176	III′
2	134	138	IV	2	134	138	IV	5	270	274	II′	5	270	274	II′
1	140	147	IV	1	140	147	IV	4	279	281	II′	4	279	280	II′
	171	173			171	174		3	282	284	II′	3	281	283	II′
4	274	278	III	5	270	271	III	2	286	305	II′	2	285	300	II′
3	280	282	III	4	273	279	III	1	weak			1	302	304	II′
2	284	287	III	3	281	282	III	4	316	318	I′	4	317	319	I′
1	290	293	III	2	284	287	III	3	weak			3	333	335	I′
				1	293	295	III	2	335	348	I′	2	336	349	I′
				4	305	306	II	1	350	334	I′	1	350	355	I′
3	311	319	II	3	311	319	II								
				2	weak		II								
1	321	336	II	1	323	337	II								
	349	351	I		350	352	I								

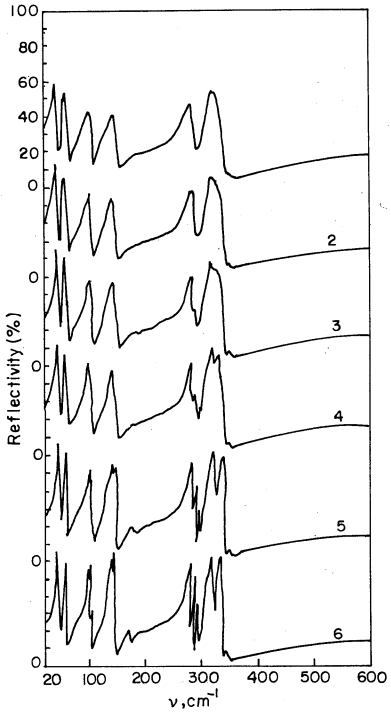


Figure 19. IR reflection spectra ($\mathbf{E} \perp \mathbf{c}$) of $TlInS_2$ for the temperatures(K) : (1) 300, (2) 220, (3) 200, (4) 180, (5) 80, (6) 6

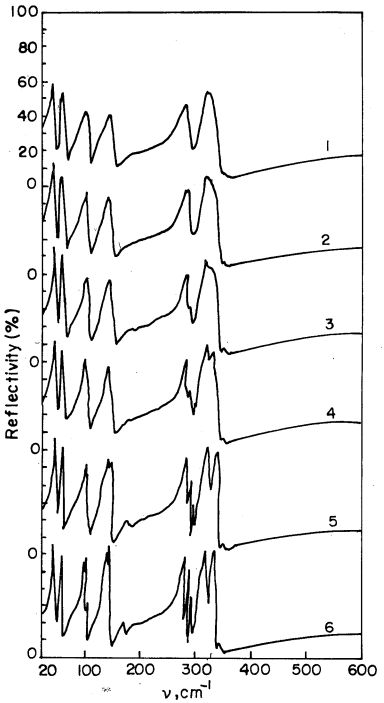


Figure 20. IR reflection spectra ($\mathbf{E} \| \mathbf{c}$) of $TlInS_2$ for the temperatures(K) : (1) 300, (2) 220, (3) 200, (4) 180, (5) 80, (6)6

Elementary vibrational model for layered (molecular) crystals gives that the unit cell doubling along the axis perpendicular to the layer surface in real space yields a double reduction of the Brillouin zone in reciprocal space. Acoustic vibrations of one-layered polytype reflected in the Brillouin zone center would result in hard interlayer vibrations of two-layered polytype, whereas optical vibrations of the zone edge reflected into the zone center would result in Davydov doublet components. Using this fact one might expect that the **c**-axis quadruplication in layered crystals provides a way of observing 4 lines instead of one. In fact, two highest-frequency absorption bands split into 4 components at low temperatures (below 170 K) for both geometries (Figures 19 and 20, curve 5, bands II and III). These bands are much more pronounced in the spectra taken at 6 K (Figures 19 and 20, curve 6).

Interpretation of the temperature variation of the polarized RS measurements, with the assumption that the space group of the crystals is C_{2h}^6 shows that a number of low temperature phase transitions exist in $TlInS_2$, as reported in Ref.[71]. For this symmetry group $10A_g$ and $14B_g$ vibrations should be expected. According to Ref.[74], A_g-type

phonons are expected for the (XX), (YY), (ZZ) diagonal components of the polarization tensor where the first and second letters refer to polarization of incident and scattered light. At the same time B_g-type phonons should be expected for (ZX), (ZY), (XZ) and (YZ) polarizations. Hence, (XX), (YY), (ZZ) spectra can be compared with (ZX), (ZY), (XZ), (YZ) spectra to distinguish between A_g and B_g-type phonons. Fig.21 gives the RS spectra for two scattering geometries, Y(XX)Z and X(ZX)Y. The spectra for X(YY)Z, Z(XX)Y, X(ZZ)X, X(ZX)Y, and Z(XZ)Y are also measured. Phonon frequencies and their symmetries are listed in Table 4. Thus it is clear that the authors of Ref.[71] observed all $10A_g$ phonons and 7 of $14B_g$ phonons predicted by the group theoretical analysis for C_{2h}^6 space group. Note that the total amount of phonons and their polarization behaviors reported in this work deny the C_s^4 symmetry group [36]. Spectral assignment based on the C_{2h}^2 group is also eliminated by small amount of the observed phonons (as compared to the symmetry theory predictions of $24A_g + 24B_g$) and by polarized IR measurements given above.

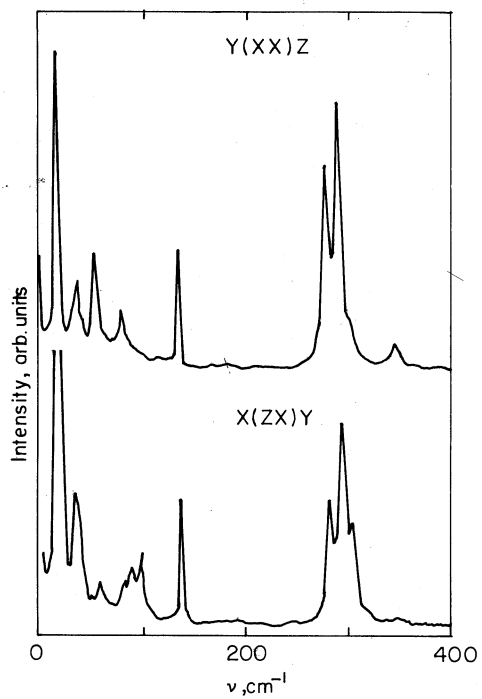


Figure 21. Raman scattering spectra of $TlInS_2$ at room temperature for two different geometries

Low-temperature features of spectral behaviors are as follows: reduction of the temperature to 240 K did not result in significant variations in the spectra recorded for

Table 4. Frequency values and symmetries of Raman active phonons in $TlInS_2$ at 300 and 12 K. Results of the other works [6, 28] are presented for comparison

13 K	110 K	12 K	300 K	300 K	300 K	
[28]	[6]	our w.	[28]	[6]	our w.	
23	22	22	19	19	19	(B_g)
28	28	27	–	–	–	
40	38	40	36	35	34	(B_g)
–	–	–	–	–	37	(A_g)
42	–	42	–	–	43	(A_g)
44	–	45	–	–	–	
47	48	49	52	51	49	(A_g)
51	–	51	–	–	–	
56	–	56	–	–	–	
59	58	59	–	–	–	
63	61	62	60	59	57	(A_g)
75	–	–	–	–	–	
81	81	79	81	81	81	(A_g)
84	–	84	–	–	–	
91	92	90	89	90	87	(B_g)
95	–	93	–	–	–	
98	100	97	100	100	98	(B_g)
105	–	101	–	–	–	
–	–	111	–	–	–	
113	117	116	–	–	115	(A_g)
–	–	–	–	125	–	
133	132	131	–	–	–	
139	138	137	138	137	137	(A_g)
270	–	268	–	–	–	
274	273	273	272	269	271	(B_g)
280	280	281	281	282	279	(A_g)
291	291	291	292	293	291	(A_g)
–	301	301	303	303	301	(B_g)
308	307	306	–	–	304	(B_g)
321	319	317	–	–	–	
326	–	319	–	–	–	
349	348	346	346	347	344	(A_g)
354	–	350	–	–	–	

different polarizations. Nevertheless, total reduction of the spectral intensity and more distinct separation of neighboring-frequency bands were typical at these temperatures. Figure 22 shows a part of the RS spectra for $TlInS_2$ taken in X(YY)Z geometry at 250 K (upper spectrum). The 17 cm^{-1} band is asymmetrical at its low-frequency wing. Spectral measurements in Y(XY)Z geometry at the same temperature (Fig.22 lower spectrum) gives the two bands (9 and 6 cm^{-1}) in the low-frequency region whose polarization behaviors conform to the B_g-type symmetry.

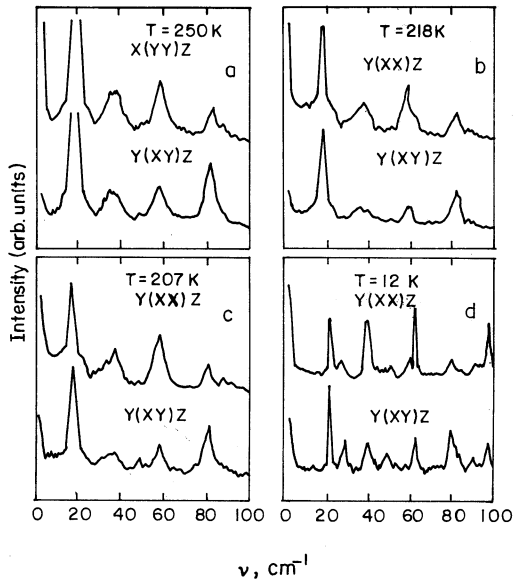


Figure 22. Low-frequency section of the Raman scattering spectra of $TlInS_2$ at various scattering geometries and temperatures

Another peculiarity of the RS spectral behavior over 218–200 K range was the detection of the two extra B_g-type bands of 7 and 10 cm^{-1} frequencies. Fig.22 gives the RS spectra between 218 and 207 K at which the crystal is in incommensurate phase [60]. Thus, the existence of low-frequency 7 and 10 cm^{-1}, B_g-type bands below 217 K seems to be due to an incommensurate phase formation followed by a lock-in transition with the quadruplication along the **c**-axis below 170 K. The band intensities markedly decreased below 168 K and they, nevertheleess, were different in the (XX) and (XY) spectra recorded at 12 K (Fig.22).

Notable variations with the temperature were observed near the 38 cm^{-1} band. As the temperature was reduced, intensity of the 38 cm^{-1} band (A in Fig.23) decreased gradually down to the temperatures 170 K. Below 170 K, two new bands appeared at the frequencies 25 cm^{-1} (C) and 30 cm^{-1} (B). Further reduction of the temperature down to 65 K resulted in the interaction of the bands A and B and merging to display a single band at 39 cm^{-1}. When the temperature dropped below 30 K the A and B components reappeared in the spectra at 40 and 42 cm^{-1} frequencies, respectively (at 12 K). Fig.24 gives the temperature variations for RS active phonons of $TlInS_2$, whose analysis yield the possible mechanisms of the observed anomalies.

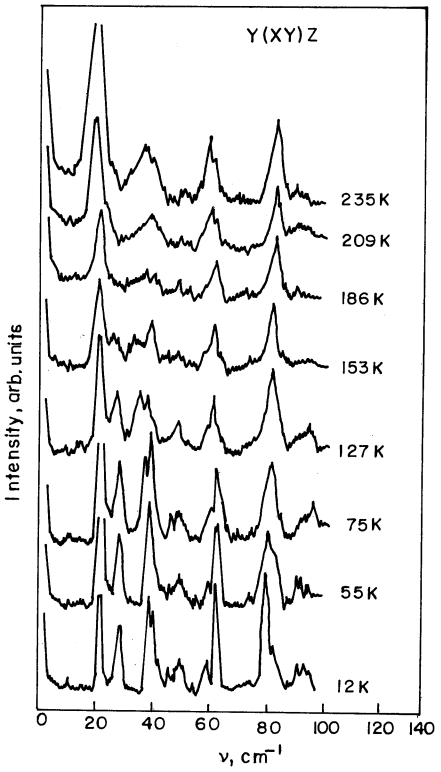


Figure 23. Low-frequency section of the Raman spectra for $TlInS_2$

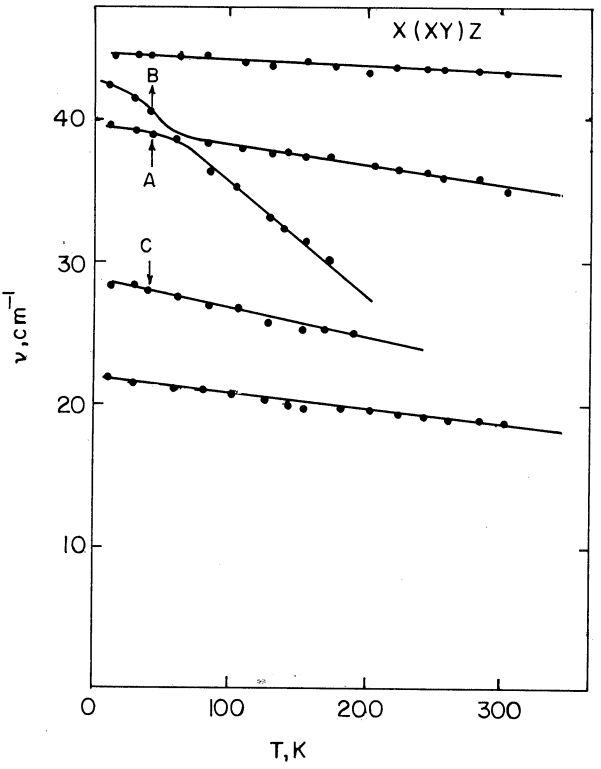


Figure 24. Temperature variation of low-frequency Raman active phonons in $TlInS_2$

Thus, the band at 42 cm^{-1} downshifts (band B for 12 K) as the temperature is increased. Temperature coefficient of the band shift $d\nu/dT = 0.08\ cm^{-1}K^{-1}$, which is larger than the similar parameter for the band at 40 cm^{-1} ($0.02\ cm^{-1}K^{-1}$). As the temperature is increased frequency intersection and phonon resonant enhancement take place in the range 55–65 K. At these temperatures both lines are represented by a single band having a peak at 39 cm^{-1}. Further increase of the temperature results in band separation, and vibration B is downshifted compared to A. In other words, vibration B acts as a soft mode whose parameters are shown in Fig.25. Square of its peak frequency is seen to be linearly dependent on temperature and may be extrapolated to zero frequency at the temperature 200 K which coincides with the jumpwise change in the temperature dependence of the soft mode ν. This suggested that the phase transition to ferroelectric state occurs at 200 K [3]. This point was also confirmed in Ref.[75] where the frequency 33 cm^{-1} was assumed to act as soft mode. Analysis of the temperature dependence of the spectra shows that the most pronounced changes can be observed over the range

160–200 K. In this range, a dramatic broadening of the B band and associated increase in the intensity decay are recorded (Fig.25). Fig.25 also shows that the frequency of the soft mode do not go to zero when the ferroelectric transition point is approached and that the soft mode overhinders within the range 160–200 K and interacts with other modes. This is supported by the RS spectra at 153, 168, 200 K (Fig.24).

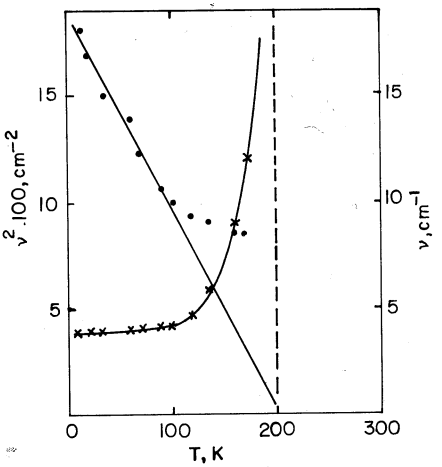


Figure 25. B band half-width (*) and square of the frequency (·) versus temperature for $TlInS_2$

It is thus apparent that the vibrational spectra of $TlInS_2$ can well be described on the basis of C_{2h}^6 space group. The presence of incommensurate phase is observed in the IR reflection spectra within the range 220–180 K by A_u-type ($\mathbf{E} \parallel \mathbf{c}$) and B_u-type ($\mathbf{E} \perp \mathbf{c}$) band activation with LO–TO splittings of 102–98 cm^{-1} and 171–173 cm^{-1}, respectively. A 42 cm^{-1} soft mode appears in ferroelectric phase at 12 K. Large amount of observed IR and RS active bands at low temperatures (80 and 12 K) are probably due to the unit cell quadruplication along the **c**-axis below 180 K and incommensurate phase formation.

Brillouin scattering investigations of $TlInS_2$ in order to get information about the dynamics of acoustic phonon modes propagating either perpendicular to the layers (C_{33} elastic coefficient) or in the layers (C_{11} elastic coefficient) were done in Ref.[76]. The samples were cut from a crystal boule grown from a stoichiometric mixture of starting materials sealed in an evacuated slica tube. The samples exhibited good optical quality and were easily cleaved into plates parallel to (001). Brillouin scattering was measured at the $\lambda = 568.2\ nm$ line of a Kr-ion laser and using a triple pass Fabry-Perot interferometer to resolve the spectra of the scattered light. In the back-scattering geometry, which was employed throughout the work, the Brillouin shift ν and the velocity v of the phonons are related as $\nu = 2nv/\lambda$, where n is the refractive index of the material. The values of

the elastic coefficients can be calculated from the expression

$$C_{ii} = \rho v_{ii}^2 = \rho \frac{\nu^2 \lambda^2}{4n_i^2}. \tag{9}$$

Here the values of the mass density $\rho = 5.71\ g/cm^3$ [76] and $n_0 = 2.54$ and $n_e = 2.37$ [77] were used. In addition to the temperature variation of C_{ii}, the interaction of the acoustic modes with other excitations can be investigated from the absorption of sound near the phase transition points. The sound absorption coefficient α is related to the full width of the Brillouin peaks at half maximum (FWHM), Γ_B, as

$$\alpha = \frac{\pi \Gamma_B}{V}. \tag{10}$$

In $TlInS_2$, macroscopical physical quantities like the permittivity or the spontaneous polarization show no anisotropy in the (001) plane [3]. This can be attributed to the similarity between the monoclinic a and b axes of the crystal as well as to the formation of a disorder twin structure in this plane [41]. Fig.26 shows the temperature variation of the elastic coefficient corresponding to the propagation of a longitudinal elastic mode with $\mathbf{q} \perp (001)$. Due to the properties of the crystal the data is related to an average elastic coefficient $C_\perp$ in this plane. The only anomaly in the temperature variation of $C_\perp$ is observed at 189 ± 2 K. This agrees with the transition temperature to an improper ferroelectric phase [3, 51].

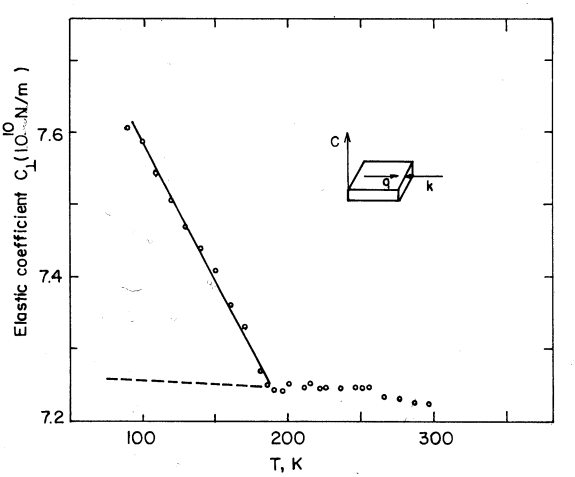


Figure 26. Temperature variation of elastic coefficient for $TlInS_2$ corresponding to $\mathbf{q} \| (001)$ longitudinal vibrations

To understand the meaning of the linear temperature dependence of $C_\perp$ below 198 K, one can use the Landau free energy expansion, which includes the coupling

terms between the order parameter q and the component of the strain, l_i. Using the approximation that the order parameter has only one component, one can get

$$F = \frac{1}{2}\alpha q^2 + \frac{1}{4}\beta q^4 + \frac{1}{2}C_{ii}l_i^2 + \gamma_i q^2 l_i + \delta_i q^2 l_i^2. \tag{11}$$

Following the standard method [14], and using the equation (11),

$$\begin{aligned} C_\perp(T) &= C_\perp^0 \qquad T > 189K \\ C_\perp(T) &= C_\perp^0 + 2\delta_\perp q^{s2} - \frac{2(\gamma_\perp + 2\delta_\perp)^2}{\beta} \qquad T < 189K \end{aligned} \tag{12}$$

can be found, where q^s and l^s are the spontaneous values of the order parameter and the strain, respectively. Since the explicit form of $l_\perp^s$ is directly proportional to q^s as can be seen from the condition $\partial F/\partial \epsilon_i = 0$

$$l_i^s = \frac{-\gamma_i q_i^{s2}}{C_{ii} + 2\delta_i q_i^{s2}}, \tag{13}$$

the significance of the third term in Eqn.(12) depends on $\gamma_\perp$. The coupling term $\gamma_i q^2 l_i$ would cause a step anamoly in $C_\perp(T)$, which is not, however, observed in the data. Secondly, the Brillouin shift does not show any anomalous temperature dependence just above the transition point, indicating that the influence of the fluctuations of the order parameter is negligible. Since the influence of the fluctuations on $C_\perp$ depends on the value of $\gamma_\perp$ [78], one can conclude that this coefficient must be small. Hence the anomalous increase of $C_\perp$ below 189 K can be attributed to $2\delta_\perp q^{s2}$, which after comparison with the experimental result gives $\delta_\perp = 1.9 \times 10^8\ N/m^2$ and $q^s \sim (T_c - T)^{1/2}$. The temperature dependence of q^s suggests that the interactions related to the appearence of the ferroelectric phase obey the mean field behavior.

The temperature dependence of C_{33}, which corresponds to the mode $\mathbf{q} \perp (001)$, is quite different than that of $C_\perp(T)$. As shown in Fig.27, there are now two clearly distinguishable anomalies at $T_1 = 213 \pm 2$ K and $T_2 = 195 \pm 2$ K. In addition, three smaller features can be observed one of which appears at 170 K. Below 195 K the increase in C_{33} can well be represented by a relation $\Delta C_{33} \sim (T_2 - T)^{2\beta}$. Straight line fits to the data, give the values $2\beta = 0.67 \pm 0.07$ and $2\beta = 0.71 \pm 0.07$ below and above the anomaly at 170 K, respectively. Actually, the best fit to the data below 170 K can be obtained by using $T_c = 190$ K instead of $T_2 = 195$ K. This suggests that the main anomaly of C_{33} in this temperature region can be attributed to the ferroelectric transition as in the case of $C_\perp$.

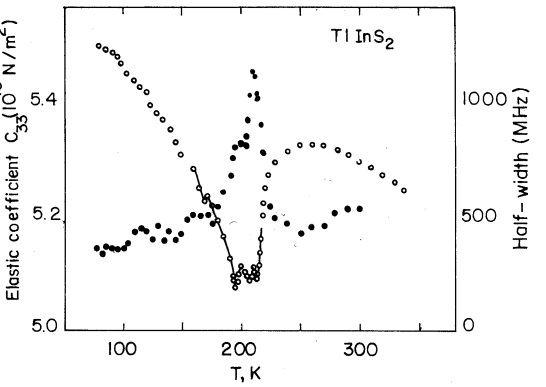


Figure 27. Temperature variation of the elastic coefficient C_{33} (open circles) and of the FWHM values of the Brillouin peaks for the mode $\mathbf{q} \perp (001)$ (dots). The solid line is to help to distinguish the weak features observed in the variation

Near the ferroelectric transition point no appreciable change of the half widths of the Brillouin peaks were found in the scattering from the mode propagating in the layer. Instead, the linewidth of the scattering peaks corresponding to the C_{33} mode exhibit clear broadining between 230 K and 175 K. This broadening has a peak at 211 ± 2 K and some poorly resolved structure on both sides of the maximum, as shown in Fig.27.

The static analysis based on Eqn.(11) can not account for the broadening of the Brillouin peaks. The shape of the function $\Gamma_B(T)$ suggests that the broadening can be attributed to a Debye relaxation process where the acoustical mode interacts with another low-frequency mode. Assuming a single relaxation process with the relaxation time t, the FWHM value of the Brillouin peak can be given in the form:

$$\Gamma_B = \frac{\mathbf{k}^2}{2\pi\rho} \frac{At}{(1 + w^2 t^2)} \tag{14}$$

where $\mathbf{k}$ is the wavevector of the phonons and A is a constant. The maximum of the broadening occurs when $wt = 1$. Attempts to fit the data to Eqn.(14) lead only to a partial success since there are three closely spaced anomalies of C_{33} between $T_1 = 213$ K and 200 K. In addition, increase of $\Gamma_B(T)$ starts well above T_1, suggesting that it can not be attributed simply to the relaxation of the order parameter at this transition. In principle, critical fluctuations could cause additional damping above T_1, but the observed anomaly in $\Gamma_B(T)$ in the temperature region $T - T_1$ is too wide for such fluctuations.

Next, IR active mode observed below $\sim 10\ cm^{-1}$ is considered [51]. This mode has singularities of ϵ' and ϵ'' at $T \sim 189$ K and $T \sim 213$ K. Between these temperatures, the dispersion of the mode changes from resonance like to relaxational one as the temperature is decreased. On the other hand, the Brillouin peaks start to broaden near temperatures where the incommensurate modulation of the lattice along the **c**-axis sets in ($T_i \sim$

216 – 220 K). In the incommensurate phase close to T_i, the modulation of the order parameter is sinusoidal. The dynamics of this plane wave regime can be charecterized in terms of amplitude and phase fluctuations, which can induce elastic anomalies in the crystal [79–81]. Actually, the IR mode which is relaxational at temperatures 189 and 213 K is attributed to the phase fluctuations of the order parameter [51]. Then the broadening of the Brillouin lines associated with the C_{33} elastic mode would result from interaction of this mode with an amplitudon and/or a phason. Along with this suggestion, observed small elastic anomalies must be related to successive changes in the modulation of the lattice when the temperature is lowered. The results of the neutron diffraction measurements [9] gave some support for this kind of modulations.

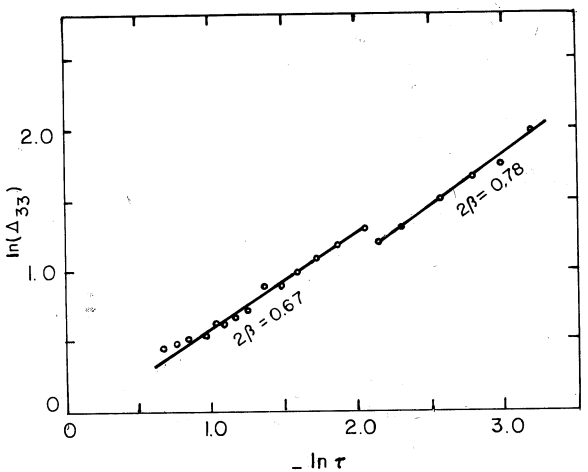


Figure 28. Logarithmic plot of ΔC_{33} vs. reduced temperature $\tau = (T_2 - T)/T_2$. The value of $2\beta = 0.71$ is obtained for $T > 170$K with $T_2 = 295$K and $2\beta = 0.67$ is for $T < 170$ K with $T_2 = 190$ K

3. Phase Transitions Under Hydrostatic Pressure

The last two decades are characterized by the vigorous development of various trends in high-pressure physics. Pressure as well as the temperature are property-establishing factors and thermodynamical parameters. A lot of data are accumulated on pressure effect on the physical properties of solids and in particular of semiconductors. Application of high pressure to solids is both simple and effective method for the alteration of their physical properties. Pressure appears to exert more effect on a solid, as compared to temperature. For instance, unit cell volume diminition by 5 percent takes place in silicon under 10 GPa, whereas temperature variation from 0 K to the melting point results in the parameter decrease by merely 1.8% [82]. For softer solids the contrast

is even more pronounced. Basically, effect of high pressure on a solid is the reduction of interatomic separation which results in the neighbouring electron orbital overlapping, crystal structure changes, energy band in the fundamental absorption edge varies, optical phonon frequency shifts, and various other effects. Property studies in solids upon interatomic separation variation give ground for interatomic coupling and intermolecular interaction theory, and for deeper insight into the lattice stability mechanism, and permit to control solid behaviours and so on. RS spectra, fundamental absorption spectra and galvanomagnetic properties of the semiconductors are of interest among the experimental high-pressure techniques of considerable current use.

Application of pressure techniques to the semiconductors with high crystal structure anisotropy showed that those experiments give much information (somewhat unique) on the electron and phonon spectral features in the substances. This is primarily true for the conductance anisotropy mechanism, the identification of rigid-layer vibrations, data on the Davydov doublets, separation between direct and indirect optical transitions (due to different rates of the band shifts upon pressure changes), assignment of polytype, etc.

The progress in optical and galvanomagnetic property studies in quasi-two-dimensional semiconductors under pressure is mainly determined by such factors as:

- Vigorous development of high-pressure technology resulting in construction of straightforward and reliable double- and triple-window optical chambers widely available for all research laboratories.

- Large progress in construction of high-sensitive electronic and optical equipments, of powerful and stable sources of coherent and incoherent radiations, thus enabling scientists to record any weak variations in the measured values under pressure.

- Progress in growth technology which resulted in crystal upgrading and extending of candidate substances whose physical properties under pressure remained undefined so far.

In this section research findings on hydrostatic pressure effect on RS and fundamental absorption spectra in layered crystals of GaSe–(A^3B^6–GaS,GaTe); $TlGaSe_2$–($A^3B^3C_2^6$–$TlInS_2$)-type structures are presented. The works on optical transmission spectra of $A^3B^3C_2^6$ crystals for pressures of up to 14 GPa are also reviewed.

The studies of pressure effect on optical properties of highly anisotropic crystals were stimulated by the polytype and rigid layer mode identifications, by the search for phase transitions under pressure, and by their potential employement as pressure gauges and calibrators. Those interested in reviews on pressure effects on optical properties of covalent and molecular crystals should refer to Refs.[82, 83].

In Ref.[82], the pressure in our investigations was exerted in a three-window fixed-pressure optical chamber. Pressure-transferring agent was dyadipat with transparent

window of 0.25 to 2.5 μm. A hydrostatic pressure of at least 1.4 GPa can be achived in this liquid at 300 K. The examinations showed that its RS spectra had no structural bands in the spectral region of interest. Spectra were excited by various lines of laser sources and recorded on the DFS12 and DFS8 double monochromators. The diffused light was collected at the right angle to the exciting radiation which strikes the fresh spall faces. The polarized Raman spectra were not studied due to the light depolarization by sapphire windows of the high-pressure chambers. All spectra were measured under pressure at room temperature. Pressure interval was 0.04–0.05 GPa for all optical experiments. Time exposure after each pressure step was at least 2 hours. Experiments were carried out also in high-pressure diamond anvil chambers with discrete pressure steps at above 1.2 GPa pressures.

Optical absorption spectra were studied by the setup based on the MDR2 monochromator with 1–2 meV resolution. Refraction coefficient variations with pressure in crystals and liquids were not taken into consideration.

From the experiments on optical phonon frequency shift by pressure the mode parameter $\gamma = (1/\nu)(d\nu_i/dP)_T$ is determined which is related to the Grüneisen parameter through

$$\Gamma_i = \frac{1}{\beta}\gamma_i, \tag{15}$$

where Γ_i is the mode Grüneisen parameter for the i^{th} phonon having frequency ν_i, and β is the isothermal compressibility. The Grüneisen parameter which determines corresponding phonon frequency variation with unit volume change reflects chemical bond nature of the crystals. In single-bond-type crystals its absolute value is independent of the phonon frequency, and for the covalent A^4 and A^3B^5 crystals Γ_i=1, for ionic-covalent A^2B^6-type crystals Γ_i=2 while for ionic crystals (alchali halides) Γ_i=3 [84]. In compounds where few bond types predominate, the Grüneisen parameter is frequency-dependent. Thus in molecular crystals with strong intramolecular and weak intermolecular bonds, the parameter Γ_i can vary from several units or even tens (for intermolecular interaction-related frequencies) to few hundredths (for intramolecular vibration frequencies). As for the layered and chain crystals with ion-covalent type bond Γ_i=1–2 should be expected for atomic vibrations inside the layers and chains, while for interlayer and interchain vibrations Γ_i should be similar to the Grüneisen parameters for interlayer vibrations in molecular crystals. In other words, studies of hydrostatic pressure effect on RS spectra in crystals enabled to estimate the interatomic and intermolecular bond nature in crystals (from the analysis of Γ_i and consequently the mode parameter value γ_i for comparison) as well as the interlayer (interchain) bond nature for layered (chain) crystals. Moreover, weak bond existence in a crystal has given the hope to discover phase transformations in such crystals under relatively moderate pressures [83].

Based on these factors the experiments on pressure effects on RS spectra of layered and chain crystals such as ϵ-GaSe, GaS, $TlGaS_2$, $TlInS_2$, $TlGaSe_2$, TlS, $TlInSe_2$, and GaTe have been initiated. The data on optical pressure studies of edge absorption spectra [84–91] and RS spectra [91, 92] have already been reported for GaSe and GaS. Subbotin et

al. [88, 89], while studying the exciton absorption spectra in ϵ-GaSe have showed that a phase transition occured under 0.43–0.47 GPa which was interpreted as an interpolytype transformation. That transformation was expected to affect RS spectra as well. However, the findings of [91, 92] cannot assist conclusively in determining the nature of RS spectra variations under pressure. Phonon frequency dependence on pressure was reported in Ref.[91], with 0.2 GPa pressure interval up to pressure of 0.6 GPa. This information was unsufficient for drawing any conclusion on phase transformation under pressure on RS spectra in ϵ-GaSe. Moreover, the problem of existence of the Davydov doublets in ϵ-GaSe RS spectra was not discussed, although both doublet components were RS-spectra active according to the selection rules [92]. Extensive experimental studies of pressure effect on ϵ-GaSe RS spectra [93] have established that the largest Grüneisen parameter of 18.7 belongs to the lowest-frequency phonon with the E-type symmetry, that occurs when the layers vibrate about each other as integral entities (interlayer vibration). According to the considerartion of Ref.[84], the intralayer vibration splitting $\Delta\nu$ having interlayer vibration frequency ν_l, can be approximately determined from the expression:

$$\Delta\nu = \frac{\nu_l^2}{\nu}. \tag{16}$$

The estimates show that the splitting varies from 1 to 3 cm^{-1} for the E-type symmetry vibrations in ϵ-GaSe. Interlayer interaction increase is to be expected with pressure growth and, consequently, splitting enhancement. In fact, differentiation of the Eqn.(16) by pressure results in

$$\frac{d\Delta\nu}{dP} = \Delta\nu(2\gamma_l - \gamma) = 2(\Delta\nu)\gamma_l \tag{17}$$

where γ_l and γ are shift parameters for interlayer and intralayer vibrations, respectively. It follows from Eqn.(16) that under pressure 1.0 GPa, intralayer vibration splitting in ϵ-GaSe would be higher by a factor of 1.5–2 than that under atmospheric pressure which as a result allows its easy observation in the RS spectra. Nevertheless, unambiguous discovery of doublets in the ϵ-GaSe RS spectra failed under high pressure. Thus, the 250 and 310 cm^{-1} doublets [92] treated earlier as Davydov doublets did not demonstrate splitting enhancement under pressure which meant that they were Davydov splitting-free. Absence of doublet structure in the other ϵ-GaSe RS bands was assumed to be associated with an extremely small intensity of one of the doublet components. It has been confirmed by the RS spectral studies at low (4.2 K) temperatures with 0.7 cm^{-1} resolution [94]. Interpolytype transformation found [85, 89] in ϵ-GaSe at 0.43–0.47 GPa does not affect the $\nu(P)$ relationships within the experimental accuracy. It is quite natural since interpolytype transformations, as a rule, insignificantly alter the crystal symmetry.

The authors of Ref.[95] determined elastic constants within the linear chain model using experimental phonon frequencies in ϵ-GaSe and GaS at various pressures, and corresponding equations given in Ref.[96]. The calculations showed that when the pressure varied from atmospheric to 1.0 GPa the interlayer interaction constants C_b^s (35%) and C_b^c (25%) (related to the layer motions about each other in perpendicular and in parallel to the

optical **c**–axis directions, respectively) underwent the greatest changes in both crystals. It should have been expected that as interlayer separation decreases with pressure (the pressure as if compresses the crystal) and results in the interaction constant to increase. Elastic constants of intermetallic interactions in ϵ-GaSe and GaS remain practically unchanged with pressure, at least up to 4.0 GPa. This fact again proves convincingly that the greatest effect on the physical processes induced by interlayer interactions in crystal are exerted by pressure.

The solution of the problem whether the lowest-frequency band (41 cm^{-1}) of the GaTe RS spectrum was related to the interlayer vibration was of interest. Additionally, pressure experiments could settle the ambiguity in the literature about the presence of the Davydov doublets in the GaTe RS spectrum.

Analysis of pressure dependences of RS active phonon frequencies in GaTe (Fig.29) excited by the 1.06 μm line of YAG:Nd^{3+} laser has established that the Γ_i parameters ($\Gamma_{i,min} = 2.2$ for $\nu = 41\ cm^{-1}$ and $\Gamma_{i,max} = 3.3$ for $\nu = 76\ cm^{-1}$ [98]) are nearly similar. This leads to the conclusion that the interlayer mode is absent in GaTe RS spectra. This observation is in agreement with the statement of Refs.[98] and [99] that the crystals have C^3_{2h} space group and their unit cell has only one layer. Before pressure experiments, the situation with the Davydov doublets in GaTe RS spectra was as follows: in Ref.[99], the RS spectra were assigned assuming the existence of the Davydov pairs in them. In Ref.[100] the doublet problem was not treated although the results were interpreted with the assumption that the unit cell has 2 layers. Baric dependence analysis from Fig.29 gives unambiguous answer to this question. Let us assume, just as the authors of Ref.[100], that RS active phonons with the 53–57; 67–76; 110–115; 153–163; 169–177 cm^{-1} frequencies form doublets. In this case, pair separations should increase under pressure of about 1.0 GPa. However, they remained actually unchanged up to 1.3 GPa within the experimental errors of Ref.[97]. Consequently, experiments on pressure RS determined that these pairs were not associated with the interlayer interaction.

RS spectra in TlS and $TlInSe_2$ crystals under pressure were excited by the 1.06 μm line of YAG:Nd^{3+} laser [101]. Previously in Refs.[102] and [103] RS active bands of TlS and $TlInS_2$ were identified by the symmetry type. The lowest-frequency vibrations of 22 cm^{-1} and 29 cm^{-1} ($TlInSe_2$) were assumed to agree with the interchain vibrations. Experiments on pressure studies of RS spectra [101] showed that these vibrations really had the largest values of frequency shifts under pressure ($\gamma_i = 10.9 \times 10^{-4}\ GPa^{-1}$ for TlS and $12.5 \times 10^{-4}\ GPa^{-1}$ for $TiInSe_2$). Shift parameters for interchain vibrations were by an order of magnitude larger than those for intrachain vibrations of A_{1g} type ($0.9 \times 10^{-4} GPa^{-1}$ and $0.3 \times 10^{-4} GPa^{-1}$ for TlS and $TlInSe_2$, respectively). Moreover, analysis of γ_i parameter conformity (lack of reference data on isothermal compressibilities prevented the Grüneisen mode parameter determinations) established that along with the weak interchain bonds some stronger intrachain bonds of ionic-covalent nature occured in the compound lattices [101]. This agreed well with the recent calculations of lattice dynamics in TlSe-type crystals based on the rigid ion model [104].

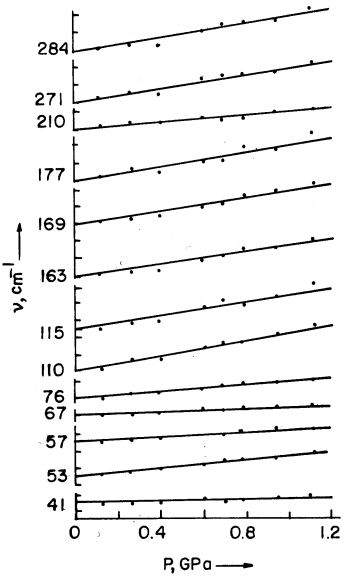


Figure 29. Raman active phonon frequencies vs. pressure in GaTe. The spectrum was excited by 1.06 μm line of the YAG: Nd^{3+} laser

RS spectra in TlS and $TlInSe_2$ crystals under pressure were excited by the $1.06\,\mu m$ line of YAG:Nd^{3+} laser [101]. Previously in Refs.[102] and [103] RS active bands of TlS and $TlInS_2$ were identified by the symmetry type. The lowest-frequency vibrations of 22 cm^{-1} and 29 cm^{-1} ($TlInSe_2$) were assumed to agree with the interchain vibrations. Experiments on pressure studies of RS spectra [101] showed that these vibrations really had the largest values of frequency shifts under pressure ($\gamma_i = 10.9 \times 10^{-4}\ GPa^{-1}$ for TlS and $12.5 \times 10^{-4}\ GPa^{-1}$ for $TiInSe_2$). Shift parameters for interchain vibrations were by an order of magnitude larger than those for intrachain vibrations of A_{1g} type ($0.9 \times 10^{-4} GPa^{-1}$ and $0.3 \times 10^{-4} GPa^{-1}$ for TlS and $TlInSe_2$, respectively). Moreover, analysis of γ_i parameter conformity (lack of reference data on isothermal compressibilities prevented the Grüneisen mode parameter determinations) established that along with the weak interchain bonds some stronger intrachain bonds of ionic-covalent nature occured in the compound lattices [101]. This agreed well with the recent calculations of lattice dynamics in TlSe-type crystals based on the rigid ion model [104].

Another peculiar feature of RS spectral behavior in A^3B^6 chain crystals under pressure was that an intensity decrease of RS active bands was detected under pressure of over 0.4 GPa ($TlInSe_2$) and 0.7 GPa (TlS). When the pressure was 0.7 GPa ($TlInSe_2$) and 0.99 GPa (TlS) or above, the intensities were so small that no RS spectra were recorded. The experiments on pressure effect on fundamental absorption edge assisted in determining the nature of the observed band intensity decreases and of the complete RS

spectra dissapearance. Baric coefficients for the band gap were $\sim$–1.58 $\times 10^{-4} eVPa^{-1}$ for $TlInSe_2$ and $\sim$–2.0$\times$ $10^{-10} eVPa^{-1}$ for TlS. Under about 0.7 GPa for ($TlInSe_2$) and 1.0 GPa for TlS, their bandgaps were estimated to diminish by 0.10 and 0.20 eV, respectively. It became evident that under the above mentioned pressures laser radiation energy ($h\nu$ =1.17 eV) was comparable to the bandgap (E_g $\simeq$1.22 eV for $TlInSe_2$ and E_g $\simeq$1.35 eV for TlS under atmospheric pressure) of the crystals considered. Last in accordance with the result that the crystals were no longer laser radiation-transparent and it was totally absorbed by a thin surface layer under these pressures and above. Since the authors of Ref.[101] employed the 90^0 geometry when recording the RS spectra under pressure no such spectra were recorded above the critical pressures.

Pioneering experiments on pressure effect on RS spectra of ternary layered $A^3B^3C_2^6$ chalcogenides were performed in 1979 [2]. The limiting pressure was 0.927 GPa for $TlGaSe_2$ and 0.726 for $TlGaS_2$. It was shown in Ref.[2] that pressure increase results not only in frequency shift but also in a new band formation in the $TlGaSe_2$ RS spectra under about 0.5 GPa. The band emergence in a narrow pressure range of (0.5–0.55 GPa) provided evidence for the phase transition occurence under these pressures. In the same pressure ranges the phonon frequency dependences on pressure showed a bending of the 54, 194, 231, and 278 cm^{-1} RS bands. A dramatic decrease in γ_i values for the four bands indicated that the interatomic bond character inside the layers alters under phase transition, and bond ionicity droped in a new phase.

The doublet emergence at 320 cm^{-1} under about 0.5 GPa deserves attention as an interesting feature of $TlGaS_2$ RS spectra under pressure. Simultaneously, a sharp reduction of all RS band strengths and a sharp decrease in the Rayleigh scattering component took place. Combination of these findings indicated that a structural phase transition occured in $TlGaS_2$ under $\sim$0.5 GPa as it was the case in $TlGaSe_2$.

The differential thermal analysis (DTA) data on $A^3B^3C_2^6$ ternary layered chalcogenides under pressure [105] and belowmentioned experimental results are the final evidences of theirs having phase transition under $\sim$ 0.5 GPa.

In all the substances under consideration [105] reversible phase transitions were found accompanied by thermal effects and characterized by the hysteresis upon inverse transition. This led to the conclusion that the phase transitions in $TlGaS_2$, $TlGaSe_2$, and $TlInS_2$ near critical pressures were first-order. Transition line slopes were determined for $TlInS_2$ and $TlGaSe_2$ as $\sim$ 160 and $\sim$ 355 K/GPa, respectively. Linear extrapolation of high-pressure transition lines on the atmospheric pressure anticipates phase transformations for $TlGaSe_2$ at $\sim$ 140 K and for $TlInS_2$, at $\sim$ 200 K. Permittivity dispersion studies described in the previous section revealed ferroelectric transitions via intermediate incommensurate phase in $TlInS_2$ near 200 K and in $TlGaSe_2$ near 110 K. Thus, similar nature of the phase trasitions recorded in the experiments under hydrostatic pressure (T=300 K) and of low-temperature transitions in ternary layer chalcogenides are not improbable.

Crystal property studies near the fundamental absorption edge is one of the sensitive optical spectroscopy methods widely employed for phase transition investigations.

Additionally, such investigations may be benefical for potential refinement of their band structures.

GaS_xSe_{1-x}, a solid solution system, forms a continuous row ($0 \leq x \leq 1$). Solutions with $x = 0.5$; 0.7; 0.8 have GaS structure (space group D_{6h}^4) . The structures of the solutions with $x = 0.4$; 0.3; 0.1; correspond either to the ϵ and γ polytypes or to their mixtures. Already early experiments on presuure effect on edge absorption spectra in GaS-type crystals ($x = 0.5$; 0.7 and 0.8) revealed a jumpwise bandgap (ΔE_g) decrease by 25 meV and 50 meV in crystals with $x = 0.5$ and x=0.7, respectively, under $P_{cr} = 1.01\ GPa$ and $1.13\ GPa$ [106, 107]. In crystals with $x = 0.5$ a hysteresis was found and $P_{cr} = 0.32\ GPa$. This finding in parallel with ΔE_g jump under P_{cr} demonstrates the presence of the first-order phase transition in crystals with $x = 0.5$ and x=0.7. One can assume that transitions observed in crystals with x=0.5 and x=0.7, and first-order phase transition in GaS under $P_{cr} \simeq 2\ GPa$ [108] have similar nature which is supported by the P_{cr} growth with sulphur concentration increase from 0.5 to 0.7 in GaS_xSe_{1-x}.

An attempt to analyze fundamental absorption spectra of GaSe-type crystals by the indirect optical transition equation was positive only for x=0.4 [106, 109]. Analysis of experimental results showed that long wavelength tail of optical absorption spectra in crystals with $x = 0.2$ and $x = 0.25$ obeyed the Urbach rule in the $90 < \alpha \leq 400\ cm^{-1}$ range and over the entire pressure range under study [110], as :

$$\alpha = \alpha_0 e^{\sigma(P)(h\nu - E_0)/kT} \tag{18}$$

where α_0 and E_0 are constants; $\sigma(P)$ is a function determining the edge tilt.

Two groups of straight lines $\ln\alpha(h\nu, P)$ are obtained for each crystal, whose convergence point coordinates (E_0, $\ln\alpha_0$) differ (see Fig.30). Such long wavelength behavior of the absorption corresponds to that predicted in Ref.[111] for the Urbach edge with phase transitions taking place in crystals when the external agent is temperature. In the present case the above mentioned experimental results showed that marked pressure range of 0.5–0.6 GPa and 0.61–0.71 GPa correspond to the phase trasition regions in $Gas_{0.2}Se_{0.8}$ and $GaS_{0.25}Se_{0.75}$, respectively.

In the context of abnormal behaviour of the Urbach rule parameters (for x=0.2 and x=0.25 crystals) similar analysis was of interest for ϵ-GaSe. As mentioned above, no common opinion on the phase transition presence in GaSe under up to 1.2 GPa was found in the literature.

The $\ln\alpha(h\nu, P)$ dependences for ϵ-GaSe is replotted using the results of Panfilov et al. [85] whose data revealed jumpwise E_0, α_0, and σ changes over the 0.35–0.44 GPa range. The fact agrees with the conclusions of Ref.[89] about the presence of phase transition in ϵ-GaSe under the pressure range 0.43–0.47 GPa. It is noteworthy that sulphur concentration increase results in P_{cr} growth from 0.44 GPa for ϵ-GaSe to 0.67 GPa for $GaS_{0.25}Se_{0.75}$. In crystals with x=0.4, transition appears for $P_{cr} > 1.2\ GPa$, i.e., beyond the technical limits of the employed optical high-pressure chamber.

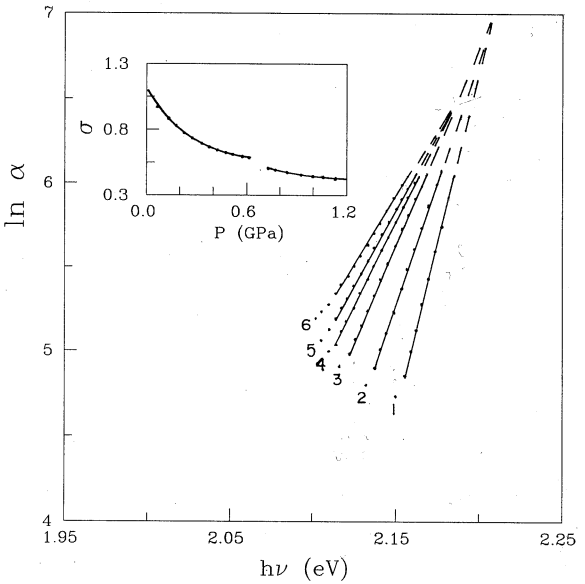


Figure 30. $\ln\alpha(h\nu, P)$ in $GaS_{0.2}Se_{0.8}$ for the pressures (GPa) : (1) 0, (2) 0.21, (3) 0.50, (4) 0.60, (5) 0.90, (6) 1.21. The insert shows pressure dependence of the parameter determining the edge tilt

Analysis of baric behaviour of edge absorption spectra of $TlGaS_2$, $TlGaSe_2$, $TlInS_2$ reported in [112–114], demonstrated that they had anomalous behaviors under 0.4, 0.76, and 0.67 GPa, respectively. In $TlGaSe_2$ and $TlGaS_2$ the anomalies show up in the rate of bandgap variation with pressure. Abnormal behaviours of electron spectra under pressure are most pronounced in $TlInS_2$ crystals. Fig.31 shows edge absorption spectra of $TlInS_2$ at certain pressures. Isoabsorption curves for different values of absorption coefficients (α) are also given in the insert of the figure. $TlInS_2$ edge absorption spectrum moves downshifts with pressure increase at the rate of:

$$\frac{dE_g}{dP} = (-8.55 \pm 0.25) \times 10^{-11} eVPa^{-1} \tag{19}$$

over the range above 0.585 GPa and over the entire interval under study. Sign of the baric coefficient for dE_g/dP, changes from negative to positive over the range 0.585 – 0.666 GPa. When $P \geq 0.756$ GPa the absorption spectrum is characterized by the emergence of a long-wave tail whose velocity shift with pressure is negative up to P_{max} = 1.044 GPa and is give as:

$$\left[\frac{dh\nu}{dP}\right]_{\alpha<30cm^{-1}} = (-20.5 \pm 0.4) \times 10^{-11}\ eV\ Pa^{-1}. \tag{20}$$

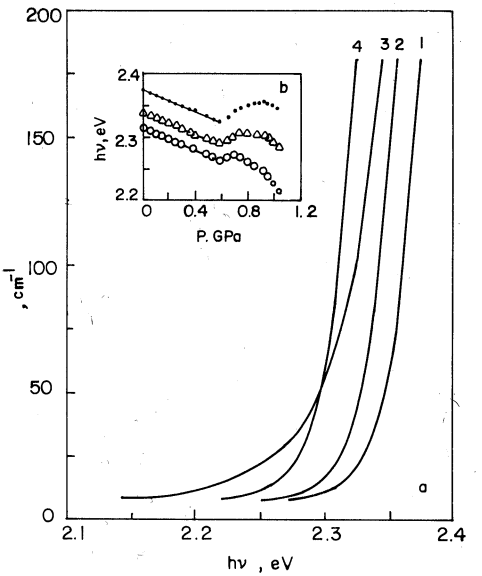


Figure 31. Fundamental absorption spectra of $TlInS_2$ at the pressures (GPa) : (1) 0, (2) 0.203, (3) 1.044, (4) 0.585. The insert shows $h\nu$ vs. P for the absorption coefficients (cm^{-1}) : 15 (o); 180 (Δ); 300 ($\cdot$)

High-energy spectral fragment is positive at least up to $\sim$ 0.903 GPa. Further pressure increase also results in a sign change for the high-energy spectral fragment ($\alpha \geq$ 90 cm^{-1}) at high pressures, as:

$$\left[\frac{dh\nu}{dP}\right]_{\alpha \geq 90 cm^{-1}} = (-11.25 \pm 0.3) \times 10^{-11}\ eV\ Pa^{-1}. \tag{21}$$

Observed behavior of $TlInS_2$ electron spectra under pressure may be due to the $TlInS_2$ phase transitions under critical pressure $\sim$ 0.6 GPa. In this case spectral transformation (upon pressure increase above P_{cr}) can be attributed to the absorption spectrum formation by two optical transitions having opposite baric coefficient signs, and to the transition pressure competetion.

In order to verify the hypothesis about the occurence of phase transition in $TlInS_2$ under pressure, relative volume variation ($\Delta V/V$) of the polycrystalline $TlInS_2$ under pressure was studied and the results were presented in Ref.[115] (curve in the insert of Fig.31). The obtained results unambiguously confirmed the presence of at least one phase transition in $TlInS_2$ under pressure at around 0.6 GPa. Stable high-pressure phase occured for $P >$ 1.05 GPa. Note that similar research on $TlInSe_2$ demonstrated transition occurence in this crystal under $P_{cr} \sim$ 0.5 GPa.

Studies of transmission spectra in $A^3B^3C_2^6$ crystals under higher pressures in the diamond-anvil cell led to new interesting results [81]. The spectra were obtained under pressure with the use of high-pressure diamond cell. The liquid used to transfer pressure was 4:1 ratio ethanol-methanol mixture which faied to produce absorption bands in the spectral region under study. The pressure in the diamond chamber was determined from the displacement of the luminescence band of 30 μm ruby crystals placed adjacent to the specimen in the chamber. The pressure measurements were done with an accuracy of ± 0.1 GPa. The spectral resolution was not worse than 4.8 nm depending on the spectral region under study, and the records were obtained using a photomultiplier (400 to 750 nm), a silicon photodiode made by the RCA company (500 to 1050 nm) and a pin germanium detector (700 to 1400 nm) cooled to 77 K. The transmission spectra of the specimens were normalized to a slit of similar dimensions by means of a minicomputer. Rate of change of the transmission coefficients with pressure ($d\tau/dP$) were determined from the transmission spectra at a 30% level. It is clear that the $d\tau/dP$ values presented in this report fail to correspond to the pressure coefficients of the direct and indirect bandgaps of the crystals studied. Nevertheless, an analysis of their variations in different pressure regions allows one to draw certain conclusions concerning the possible existence of phase transitions under pressure which were not observed before. The results were as follows:

$TlGaS_2$ – Figure 32 gives the room temperature transmission spectra of a 20 μm-thick $TlGaS_2$ crystal under different pressures. The pressure dependence of the transmission coefficient (at a 30% level) of a $TlGaS_2$ crystal is depicted in Fig.33. The analysis of the spectra and the baric coefficients have shown that there are pressure regions with different behaviors of the displacement transmission coeffcicients. It has different magnitudes for different pressure ranges and even sign changes were observed in some of the regions. These pressure ranges and the corresponding baric coefficients are:

Phase	Pressure range (GPa)	Baric coefficient $d\tau/dP$ (eV/Pa)
I	0 – 0.8	$(3.7 \pm 0.2) \times 10^{-11}$
II	1.2 – 3.13	$(-13.2 \pm 0.2) \times 10^{-11}$
III	3.13 – 5.027	–
IV	5.027 – 8.22	$(-7.23 \pm 0.2) \times 10^{-11}$

Above 3.13 GPa the crystal color varied from light yellow to dark red, and in the pressure region from 3.13 to 5.027 GPa a severe variation of transmission spectra was observed and some crystals collapsed, which made difficult to determine the displacement transmission coefficient at a 30% level. A sharp variation of the spectra in the 3.13 to 5.027 GPa region allows one to suppose the existence of a phase transformation in $TlGaS_2$ crystals above 3.13 GPa and the formation of a new stable high-pressure phase above 5.027 Gpa, that exhibits stability up to ~ 8.22 GPa. In the transitional pressure regions

(from 0.8 to 1.2 GPa and from 3.13 to 5 GPa) the existence of different phases is possible. In the reverse direction (when the pressure is decreased) of the transmission spectra, a ~ 0.15 GPa pressure based hysteresis was observed with all of the three areas of spectral dependences on pressure, which allows one to suppose that the phase transformations observed in the $TlGaS_2$ crystal may be classified as the first order transformations. This is also supported by the results of a differential thermal analysis of $TlGaS_2$ crystal under pressure[105].

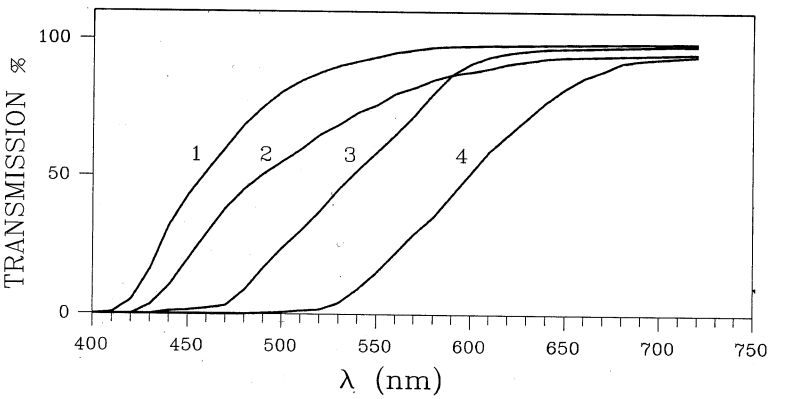


Figure 32. Transmission spectra of 20 μm-thick $TlGaSe_2$ at room temperature for the pressures (GPa) : (1) 0.164, (2) 1.932, (3) 5.027, (4) 8.219

$TlGaSe_2$ – Reference [114] presented a rather complete analysis of the displacement of the indirect absorption edge in the pressure region of up to 1.274 GPa. It was noted that a stabilization of the displacement transmission coefficient of the indirect absorption edge of crystals was observed in the pressure region above 0.915 GPa. The experiments performed make it possible to analyze reliable the pressure dependence of the transmission spectra of $TlGaSe_2$ crystals in the pressure region of up to 14.82 GPa.

Figure 34 gives the transmission spectra of a $28\mu m-$thick $TlGaSe_2$ crystal under pressures at room temperature. Figure 33 (curve b) exhibits the baric dependences of the transmission coefficient (at 30% level). It is seen that three regions with different displacement coefficients can be singled out in the pressure region under study:

Phase	Pressure range (GPa)	Baric coefficient $d\tau/dP$ (eV/Pa)
I	$0 - \sim 1$	–
II	1.85 – 4.35	$(-19.2 \pm 0.2) \times 10^{-11}$
III	5.652 – 8.515	$(-7.9 \pm 0.2) \times 10^{-11}$
IV	9.761 – 14.82	$(-6.1 \pm 0.2) \times 10^{-11}$

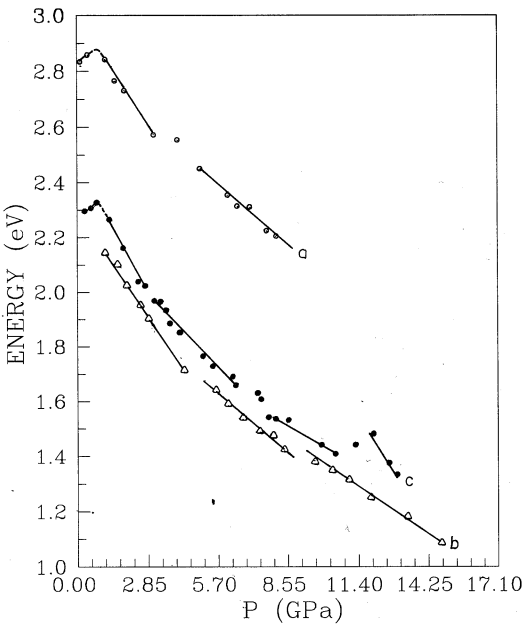


Figure 33. Crystal transmission factor vs. pressure at room temperature for (a) $TlGaS_2$, (b) $TlGaSe_2$, (c) $TlInS_2$

In the transitional pressure regions (of $\sim$ 0.8 to $\sim$ 1 GPa, $\sim$ 4.35 to $\sim$ 5.7 GPa, and $\sim$ 8.5 to $\sim$ 9.7 GPa) coexistence of different phases is possible. As in $TlGaS_2$ crystals, a $\sim$ 0.25 GPa pressure-based hysteresis is observed in all areas of reversed spectra, which allows one to suppose that the phase transformations observed in the $TlGaSe_2$ crystal can be classified as the first-order one. The hysteresis value in the $TlGaSe_2$ crystal (0.25 GPa), as compared to that of 0.15 GPa in the $TlGaS_2$ crystal, shows evidences for the fact that in a $TlGaSe_2$ crystal exposed to pressure, the phase transformations are more pronounced. This fact was also proved by the differential thermal analysis of ternary layer chalcogenides under pressure [105].

$TlInS_2$ – Reference [113] presented absorption spectra of $TlInS_2$ crystals exposed to pressures of up to 0.801 GPa at room temperature. According to Ref.[114], the pressure coefficient of the bandgap (determined from the pressure dependences of the absorption coefficients below 30 cm^{-1}) in the pressure region of up to 0.585 GPa was: $dE_g/dP = (-8.55 \pm 0.25) \times 10^{-11} eV/Pa$. In the pressure region above 0.903 GPa [114] a sign reversal of the baric coefficient took place, and the folowing values were determined at different absorption coefficients:

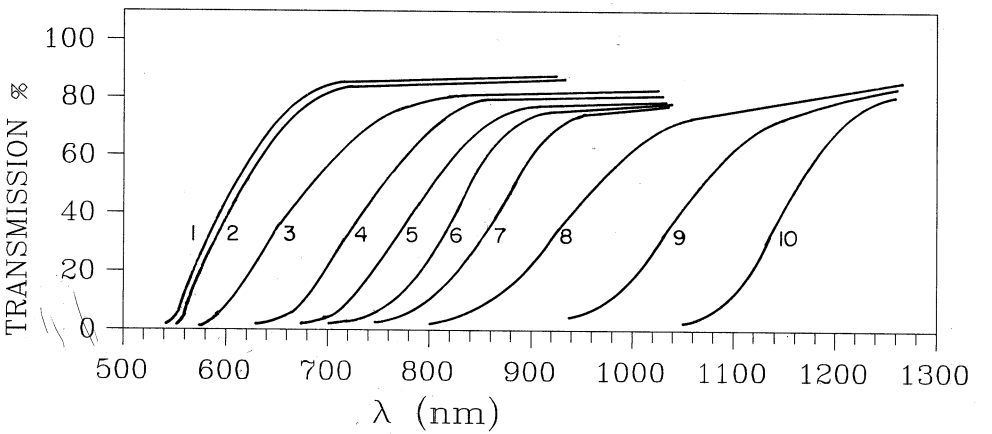


Figure 34. Transmission spectra of 28 μm-thick $TlGaSe_2$ at room temperature for the pressures (GPa) : (1) 1.09, (2) 1.47, (3) 2.67, (4) 4.35, (5) 5.65, (6) 6.86, (7) 7.91, (8) 10.32, (9) 13.49, (10) 14.82

$$\left[\frac{d(h\nu)}{dP}\right]_{\alpha<30cm^{-1}} = (-20.5 \pm 0.4) \times 10^{-11} eV\ Pa^{-1}, \quad (22)$$

$$\left[\frac{d(h\nu)}{dP}\right]_{\alpha\geq 90cm^{-1}} = (-11.25 \pm 0.3) \times 10^{-11}\ eV\ Pa^{-1}.$$

Figure 35 depicts the transmission spectra of a 25 μm-thick $TlInS_2$ crystal under different pressures at room temperature. Measurements made it possible to analyze reliably the baric dependences of crystal transmission spectra in the pressure region of up to 13.11 GPa. The baric dependences of the transmission coefficient (at 30% level) are given in Fig.33 (curve c). It can be seen that five regions with different displacement coefficients can be identified and the corresponding values of the baric coefficients are as follows:

Phase	Pressure range (GPa)	Baric coefficient $d\tau/dP$ (eV/Pa)
I	$0 - \sim 1$	$(4.7 \pm 0.2) \times 10^{-11}$
II	1.0 – 2.85	$(-12.9 \pm 0.2) \times 10^{-11}$
III	3.37 – 6.3	$(-9.3 \pm 0.2) \times 10^{-11}$
IV	7.64 – 10.6	$(-7.2 \pm 0.2) \times 10^{-11}$
V	12.10 – 13.11	$(-15.9 \pm 0.2) \times 10^{-11}$

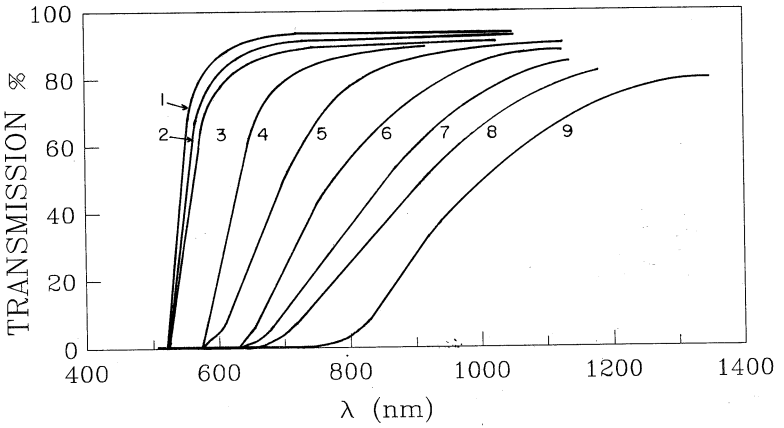


Figure 35. Transmission spectra of 25 μm-thick $TlInS_2$ at **room temp**erature for the pressures (GPa) : (1) 0.23, (2) 0.822, (3) 1.347, (4) 2.433, (5) 3.8, (6) 5.167, (7) 6.3, (8) 7.64, (9) 9.963

Since there were few experimental points between 10.6 and 12.10 GPa pressure region, it was difficult to determine the sign and the value of the baric coefficient in this region. Nevertheless, the possibility of its sign reversal to positive again is not ruled out.

In the intermediate pressure regions (from ~ 2.85 to ~ 3.37 GPa, from ~ 6.3 to ~ 7.64 GPa, from ~ 10.6 to ~ 12.10 GPa) the existence of different phases is possible. As in $TlGaS_2$ and $TlGaSe_2$ crystals, a pressure-based hysteresis is also observed at ~ 0.3 GPa in $TlInS_2$, which makes it possible to suppose that the phase transformations observed in the crystal can be classified as a first-order transitions.

Thus, the results of the study show that the $A^3B^3C_2^6$ ternary layered chalcogenides undergo a number of phase transformations under high pressures. This makes them interesting materials to study the physical properties at high pressures and allows one to hope to use them as reference materials in high-pressure technology.

Interesting results are obtained using the temperature dependences of dielectric properties, conductivity and spontaneous polarization of various sets of $TlInS_2$ crystals as well as of the influence of hydrostatic pressure up to 0.8 GPa on the anomalies of these properties.

In Ref.[116], specimens of size $5 \times 2 \times 1.5$ mm^3 were used in the measurements. Since no anisotropy of the dielectric properties was observed in the direction along the (001) plane, electrodes were placed on to the surface in the direction perpendicular to the layer plane. Vacuum deposited silver was used as electrodes. The measurements were carried out at the frequencies 110 GHz and 1 kHz by Ando alternating current bridges TR-10C and E7-8, within the temperature range 100–300 K with accuracy ± 0.02K. The measurements were taken in a self contained high pressure chamber. A detailed description of the technique is given in Ref.[117]. A mixture of isopentane and transformer oil was used as the pressure transfering agent. The spontaneous polarization was deter-

mined by the loops of the dielectric hysteresis, which were measured using the modified Sawyer-Towers scheme at 50 Hz frequency.

Figure 36 shows some typical variations of the permitivity $\epsilon_\alpha(T)$ with the temperature measured for one of the specimens at various pressure[1] In addition to the anomalies observed at atmospheric pressures (commensurate at $T_i = 214$ K and ferroelectric at $T_f = 202$K [3]) extra anomalies were observed in $\epsilon(T)$. At these temperatures, anomalies in the heat capacity [118, 119], optical properties and the coefficient of thermal expansion were also observed for $TlInS_2$. Anomalies in the absorption of longitudinal ultrasound wave were reported [120]. The character of these anomalies and their reproducibility at repeated intervals show that they correspond to the phase transitions as given in Fig.37 and in Tables 5 and 6.

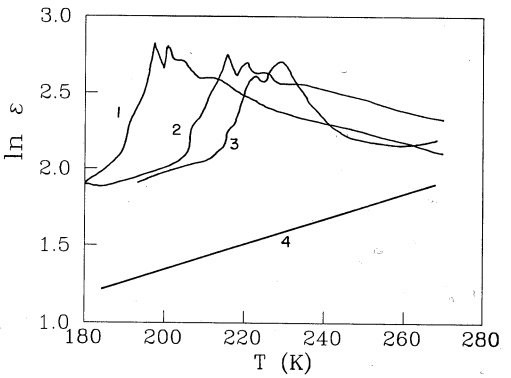


Figure 36. Quasi-isobaric temperature variation of ϵ_α for $TlInS_2$ for the initial pressures (GPa) : (1) 0, (2) 0.5, (3) 0.69, (4) 0.79

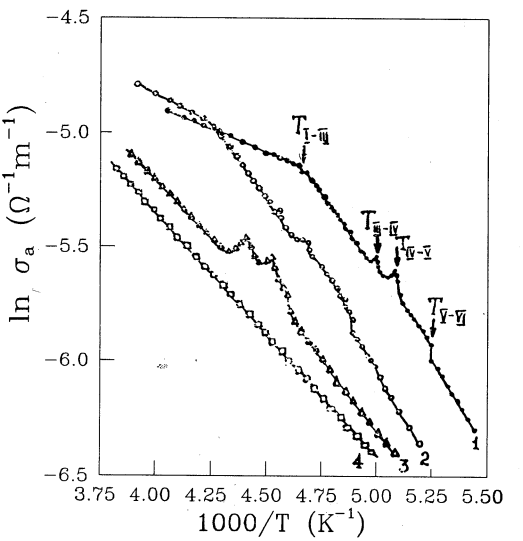


Figure 37. Quasi-isobaric temperature variation of the conductivity σ_α for $TlInS_2$ for the initial pressures (GPa) : (1) 0, (2) 0.5, (3) 0.69, (4) 0.79.

The measurements of spontaneous polarizations (P_s) by the loops of dielectric hysteresis did not permit to draw a certain conclusion on the temperature at which P_s originates since during the phase transitions III–IV and IV–V the induced polarization considerably exceeded the spontaneous one. One can draw a mere conclusion on the nature of these phase transitions analyzing the temperature dependencies of the imaginary part of the permittivity ϵ'' or conductivity σ. The conductivity measured at alternating current can be determined using the expression $\sigma = \epsilon''\epsilon_0 w + \sigma_p$ where ϵ_0 is the electric constant;

[1] In fact, The temperature variation of ϵ_α given in Fig.36 and the variation of $log\sigma_\alpha(1000/T)$ given in Fig.37 are quasi-isobaric since in this technique the pressure is decreased as the temperature of the chamber is decreased.

w is the external field frequency and σ_p is the through conductivity of the specimen (in $TlInS_2$, the conductivity is p-type).

Table 5. Conductivity activation energies (ΔE_i) for various phases.

Phase	ΔE_i (eV)
I	0.08 ± 0.01
II	0.21 ± 0.01
III	0.27 ± 0.01
IV	0.27 ± 0.01
V	0.27 ± 0.01
VI	0.31 ± 0.01

Table 6. Phase transition temperatures at $P = P_0$, and the corresponding isobaric coefficients.

Phase transition	$T_{tr}(P = P_0)$ (K)	dT_{tr}/dP (K/GPa)
I–II incommensurate	213.5	58.8
III–IV ferroelectric	201.5	51.1
IV–V ferroelectric	198.0	48.9
V–VI ferroelectric	192.0	41.3
I–II structural	–12.3	435

In the vicinity of the ferroelectric 2^{nd} order phase transition dielectric losses and consequently ϵ'' increases abnormally, whereas in the structural phase transition the dielectric losses remain the same; however, only the parameters which determines the through conductivity of the crystal, in particular the activation energy ΔE_i, changes. In Fig.37, which shows the dependences $\log\sigma_\alpha(1000/T)$ measured at 1 kHz frequency at various initial pressures, one can see that at the incommensurate phase transition I–III, there is a break in the temperature dependence of σ_α constructed in the Arrhenius coordinates (The values of ΔE_i for different phases are given in Table 5). On the other hand, in the vicinity of the phase transitions III–IV and IV–V the conductivity increases abnormally which can be interpreted as ferroelectric phase transitions. It should also be noted that the activation energy (ΔE_i) hardly changes at these transitions (Fig.37). Phase transitions I–III, III–IV and IV–V are the second order, whereas the jumps in ϵ_α and σ_α at $T = T_{V-VI}$ and a small temperature hysteresis ($\sim 0.5^0$) show that the transition V–VI is first order.

As the pressure rise up to $\sim 0.6\ GPa$, the shapes of the anomalies in $\epsilon_\alpha(T)$ and $\sigma_\alpha(T)$ does not change qualitatively (Figs.36 and 37), but only a temperature rise of

phase transition is observed. The isobaric $1/\epsilon_\alpha(T)$ and isothermic $1/\epsilon_\alpha(P)$ dependences (Fig.38) were calculated for qualitative analysis of the obtained experimental data for the influence of pressure on the dielectric properties $\epsilon_\alpha(P,T)$ of $TlInS_2$, taking the pressure change in the chamber into account at decreasing temperature. At $P \leq 0.6GPa$ and within temperature ranges $T - T_{I-III} \leq 40^0$ and $T_{III-IV} - T \leq 8^0$, these variations can well be approximated by Curie-Weiss laws:

$$\epsilon = \frac{C^+}{T - T_0^{\pm}(P)}, \quad P = constant \tag{23}$$

$$\epsilon = \frac{C_p^{\pm}}{P - P_0^{\pm}(T)}, \quad T = constant \tag{24}$$

where $C^{\pm}$ and $C_P^{\pm}$ are the Curie constants for isobaric and isothermic dependencies of permittivity in I-paraelectric (C^+) and V-ferroelectric (C^-) phases and $T_0^{\pm}(P)$ are the Curie-Weiss temperatures and the temperatures obtained by extrapolating the corresponding dependences to the values $1/\epsilon = 0$ (Fig.35).

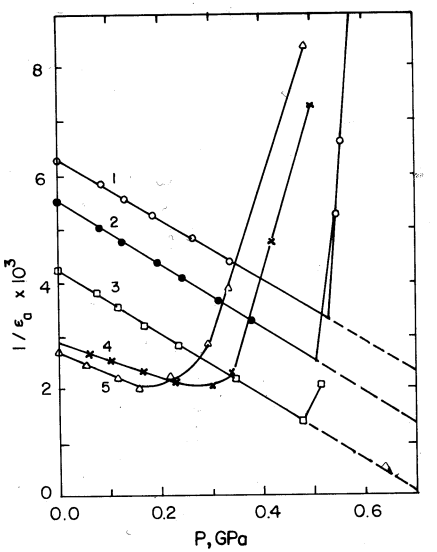


Figure 38. Permittivity (ϵ_α) vs. pressure in $TlInS_2$ for the temperatures (K) : (1) 254.4, (2) 242.5, (3) 228.4, (4) 214.4, (5) 210.5

Constants C and C_P do not depend on the pressure and the temperature within the experimental error and have the values : $C^+ = (1.23 \pm 0.05) \times 10^4$ K, $C^- = (2.2 \pm 0.1) \times 10^3$ K, $C_P^+ = (1.7 \pm 0.1) \times 10^2$ GPa, $C_P^- = (33 \pm 1)$ GPa.

At the pressure of $P \geq 0.6$ GPa a sharp decrease of permittivity and conductivity of $TlInS_2$ (Fig.39) is observed which shows the presence of another phase transition I–II.

This is a first order transition which is close to the second order one. Pressure hysteresis does not exceed 0.01 GPa. As the temperature is decreased the permittivity and the conductivity at phase II decrease monotonously (curves 4 of Figs.36 and 37). Increase of conductivity with pressure in phase I and its decrease in phase II correlate with the change of sign in the baric coefficient of the bandgap at this phase transition detected in Ref.[114].

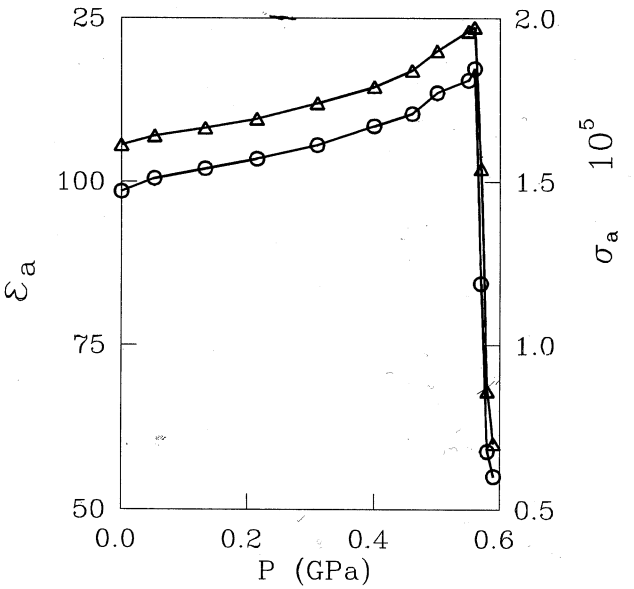


Figure 39. Permittivity (ϵ_α) and conductivity (σ_α) vs. pressure in $TlInS_2$ at the temperature 260 K

Figure 40 shows the phase diagram (PT–diagram) of $TlInS_2$ constructed on the basis of $\epsilon_\alpha(T,P)$, $\sigma_\alpha(T,P)$ dependences. As the pressure is increased the temperatures of the phase transitions I–III, III–IV, IV–V, V–VI linearly increase. The values of the baric coefficients dT_{m-n}/dP are given in Table 6. As it is seen, these values decrease monotonously as T_{m-n} is decreased, independent of the fact that the phase transition is incommensurate or ferrolectric.

Unlike the rest of phases, phase II is stable at the pressures $P \geq 0.5\ GPa$ since the phase transitions I–II, III–II, IV–II, V–II, and VI–II are characterized by very large positive baric coefficients (Table 6 and Fig.40). The lines of these phase transitions intersect with those of commensurate and ferroelectric phase transitions at triple points. However, we succeeded to determine accurately the coordinates only for the triple point in which phases I, II, III are in equilibrium: $P = 0.54\ GPa$; $T = 245$ K.

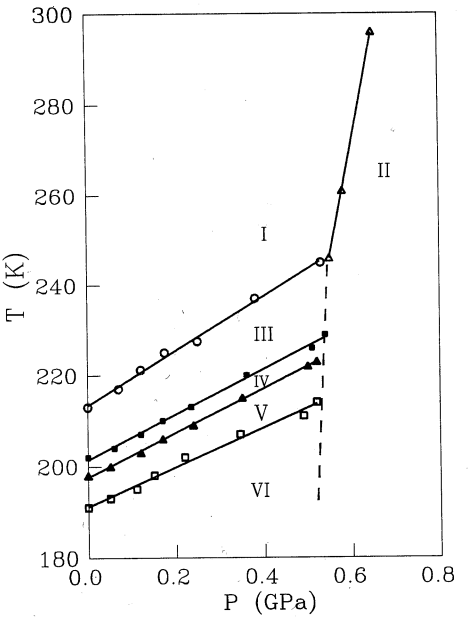


Figure 40. $TlInS_2$ phase diagram $(P-T)$

In the other specimens some of the above mentioned anomalies were not observed or, on the contrary, additional weak anomalies appeared. These differences should be connected evidently with the polytypism characteristic for $TlInS_2$ [54, 121].

Analyzing the experimetal data for different specimens systematically allowed to divide them into three groups as follows :

- The specimens whose permittivity in the plane (001) follows the Curie-Weiss law in the paralectric phase (Curie constant is $5\times10^3 K \leq C \leq 1.2\times10^4$ K) and there is an incommensurate phase ($T_i = 214 \pm 1$ K) as well as a multiple of successive ferroelectric phase transitions at $180K \leq T \leq 206$ K (Figures 41 and 42, curves 1).

- The specimens whose permittivity in the plane (001) follows the Curie-Weiss Law ($C \simeq 10^3$ K). There are 2–3 successive phase transitions without an incommensurate phase (Figures 41 and 42, curves 2).

- The specimens in which the Currie-Weiss law for the temperature dependence of $1/\epsilon_\alpha$ is not followed and there is no incommensurate phase but 2–3 ferroelectric phase transitions occur between 198 K $\leq T \leq$ 206 K (Figures 41 and 42 curves 3).

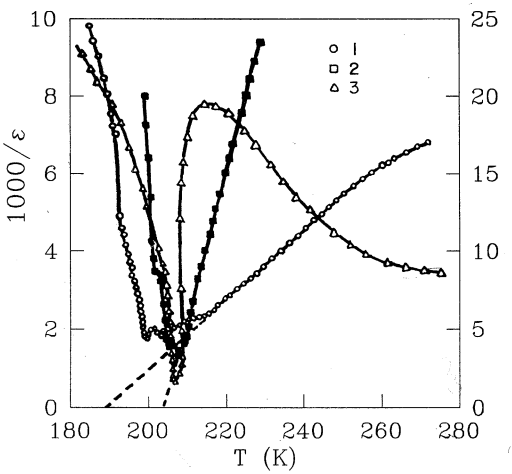


Figure 41. Inverse temperature variation of the permittivity for various specimens : (1) first group specimens (100 kHz), (2) second group specimens (100 kHz), (3) third group specimens (110 kHz)

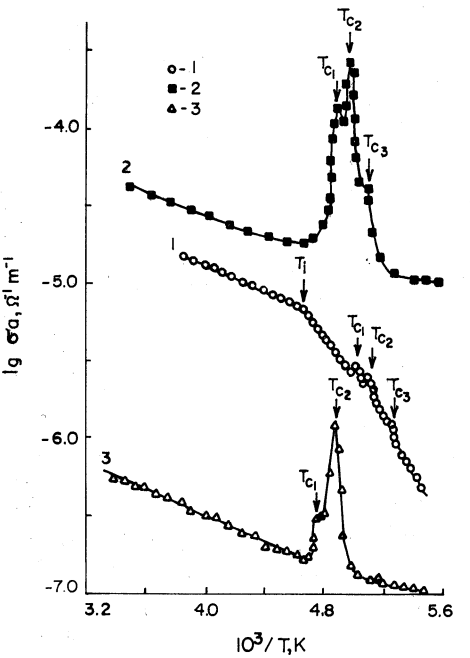


Figure 42. Temperature variation of the conductivity for various specimens : (1) first group specimens (100 kHz), (2) second group specimens (100 kHz), (3) third group specimens (110 kHz). Points of incommensurate and ferroelectric phase transitions are marked by arrows

Thus, two assumptions can be made for the reasons of the above differences between the properties of the specimens and successive phase transitions in $TlInS_2$ crystals. First one is that the specimens are uniform by volume and belong to three different polytype modifications. The second assumption is that specimens are non-uniform mixtures of different volume fractions of polytypes.

For a more unambiguous conclusion one of the 2nd group specimens was measured with gradual size reduction (l_c) in the direction of the **c**-axis. The results of these measurements are given in Fig.43 and in Table 7. As it can be seen, when l_c is decreased the shape of the anomalies in the temperature variation of ϵ_α as well as their number and temperatures change. Moreover, at $l_c = 0.36\ mm$ a weak anomaly at $T_i = 214$ K appears corresponding to the incommensurate phase transition. This result confirms the assumption that the group 1 and 2 specimens are a mixture of various poytypes with

different volume fractions. But this result does not exclude the presence of several phase transitions in some of the polytypes.

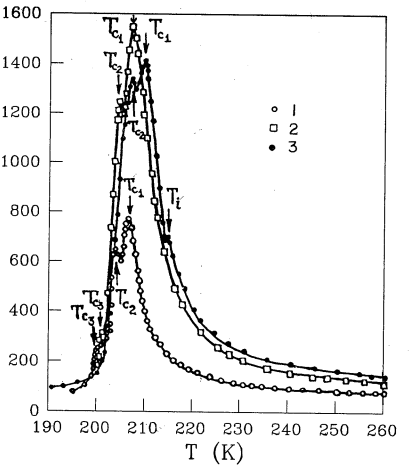


Figure 43. Temperature variation of the permittivity for the second group of $TlInS_2$ specimens along the **c**-axis for the specimen sizes (mm) : (1) 0.82, (2) 0.42, (3) 0.36

Table 7. Temperatures of incommensurate (T_i) and ferroelectric (T_{ci}) phase transitions in the second group specimens with various thicknesses, l_c, in the **c**-axis direction.

$l_c(mm)$	T_i(K)	T_{c1}(K)	T_{c2}(K)	T_{c3}(K)
0.82	–	206.0	203.6	200.0
0.42	–	206.4	204.1	200.8
0.36	214	209	206.5	202.4

The temperatures of all anomalies increase linearly under the action of hydrostatic pressure. One should note that the value of the baric ocefficient is proportional to the temperature of the anomaly but independent of weather this anomaly corresponds to a basic phase transition or an additional weakly marked ferroelectric transition. Similar decrease of the baric coefficient with the temperature of the anomaly was observed in the polytype ferroelectric $K_4Fe(CN)_6 \cdot 3H_2O$ [122].

The presence of the soft relaxation type optical mode in $TlInS_2$ crystals [51] and of the value of the Currie constants show that the phase transitions in $TlInS_2$ are "proper" order-disorder transitions in terms of the microscopic theory [123]. This conclusion does not contradict the results obtained in an earlier work [95]. To see this, let us write the thermodynamic potential in this case, without taking into account the incommensurate

phase as:

$$\Phi = \frac{1}{2}4\pi\left(\frac{T-T_0}{C}+QP\right)P^2+\frac{1}{4}\beta P^4 - PE \tag{25}$$

where Q is the electrostriction constant, β is the coefficient independent of P and T, E is the external field, T_0 is the Curie-Weiss temperature at $P = P_0$. Then, it is easy to derive equations (23) and (24) using the Eqn.(25), and moreover, $T_0(P)$ and $P_0(T)$ can be determined by the utility of thermodynamic potential coefficients given by Eqn.(25) as

$$T_0(P) = T_0 + QC_P P, \tag{26}$$

$$P_0(T) = -\frac{T-T_0}{QC}. \tag{27}$$

The correlation between the constants C and C_P is

$$\frac{C}{C_P} = \frac{dT}{dP}. \tag{28}$$

Considering the fact that dT_0/dP coincides with dT_{III-IV}/dP, within the experimental error, one can calculate the values of C_p^+ and C_P^- using equation (27) and the constants C^+ and C^- derived in section 2 for one of the specimens. Using such calculations we can obtain the values $C_P^+ = 2.4 \times 10^3\ GPa$ and $C_P = 43\ GPa$, which are in good agreement with the experimental values of $C_P^+ = 2.2 \times 10^3\ GPa$ and $C_P^- = 33\ GPa$ obtained for this specimen.

On the other hand, since according to Ref.[60] the incommensurate phase is characterized by the wavevector $\mathbf{k}_i = (\delta;\delta;0.25)$ the cell volume in the direction of **c**-axis should increase by four times which means that the ferroelectric phase transition should be improper. Besides, the correlation that should be satisfied for the "order-disorder" phase transition [123]:

$$C = \frac{4\pi P_S^2 V}{k} \tag{29}$$

where P_S is the saturated value of the spontaneous polarization, V is the volume of the unit cell, k is the Boltzmann constant.

In the specimens of $TlInS_2$ under study, P_S did not exceed $0.35\mu C/cm^2$. If this value is substituted in Eqn.(12) one can obtain $C = 6$ K which is three orders of magnitude less than the experimental values of C^+ and C^- . This fact also shows that the ferroelectric phase transitions in these crystals are improper. Thus, the available experimental data do not allow to draw an unambigous conclusion on the nature of the incommensurate and ferroelectric phase transitions.

Evidently, most β-$TlInS_2$ crystals are a mixture of polytypes so that some of these polytypes undergo both incommensurate and ferroelectric phase transitions while others undergo only ferroelectric ones.

4. Optical Transmission, Conductivity and Hall Effect Under Pressure in TlSe-type Crystals

The investigations of the electron spectra of Tallium Selenide-type (chain structure) semiconductors, TlSe, $TlInSe_2$, $TlInTe_2$, revealed no anomalies in the bandgap variation with the pressure up to 0.6 GPa [124–126]. The results obtained in these works agree qualitatively with the theoretical calculations of the band structure for this type of semiconductors [127]. For the A^3B^6 chain semiconductors the baric coefficients of direct and indirect band edges are also determined, which decrease linearly with the pressure at the rates :

	$dE_g^i/dP(eV/Pa)$	$dE_g^d/dP(eV/Pa)$
TlSe	-2.0×10^{-10}	-1.25×10^{-10}
$TlInSe_2$	-1.5×10^{-10}	-1.1×10^{-10}
$TlInTe_2$	-2.0×10^{-10}	-1.0×10^{-10}

The difference of the values of the indirect edge dE_g^i/dP in $TlInSe_2$ compared to the values for TlSe and $TlInTe_2$ allows to assume that the minimal energy gap in these crystals is of different origin. This assumption does not contradict the calculations of the energy band structure of the thallium selenide type crystals [127] testifying to the presence of a number of nearby indirect transitions from T_3 point of the valence band to the nearby minima D_1, A_4, Σ_1, Δ_1 of the conduction band and is confirmed by the difference of low-temperature optical spectra of TlSe, and $TlInTe_2$, on the one hand, and of $TlInSe_2$, on the other hand, in the region of their indirect edge [128, 129].

Anisotropy of the electrical conductance and Hall effect of TlSe crystals under pressure was studied by the authors of [130]. They presented the results of experimental study of the hydrostatic pressure pressure influence (up to 0.84 GPa) on the anisotropy of the conductivity and of Hall constant of n-TlSe crystals at room temperature. From the analysis of temperature dependences $\sigma_{\|}$ and $\sigma_{\perp}$ (in the region of 200 to 300 K at atmospheric pressure) conductivity activation energy values were determined. Experimental values of the baric coefficients of conductivity activation energy are obtained for the passage of current in two mutually perpendicular directions. It is established that with the increase of pressure and temperature the anisotropy of electrical conductance decreases. It is shown that the basic features of kinetic effects in TlSe are qualitatively explained within the framework of the conductivity and Hall effect of the inhomogenous crystal.

The crystals for investigations were grown by the Bridgman technique. Synthesized product was preliminary cleaned by the horizontal melting method. The lowest concentration of the current carriers $n_o = 3 \times 10^{14}\ cm^{-3}$ (at room temperature and atmospheric pressure) was reached by multiple passages (not less than 10 passages) through the melted zone. The carrier type was determined by measuring the Hall effect. In the case $\mathbf{J} \| \mathbf{c} \perp \mathbf{H}$ the carrier type corresponded to p-type, in the case of $\mathbf{J} \perp \mathbf{c} \| \mathbf{H}$ it was n-type. Hereafter

J is the direction of current, **c** is the direction of optical axis coinciding with that of the crystal tetragonal Z-axis, **H** shows the direction of magnetic field applied to the specimen.

The measurements under pressure were carried out in high-pressure beryllium bronze chamber by the compensational technique with direct current. Dewatered mixture of the transformer oil and kerosene (1:4) served as pressure-transfering agent. The pressure was measured using the calibrated manganin manometer to an accuracy of 1%. After the next pressure was established some changes of the measured parameters in time was observed (2–3 hours), as a result the crystal was exposed under the fixed pressure not less than 5 hours which guaranteed that the measurements were carried out in the equilibrium conditions. The ohmic capacity of contacts was controlled by measuring the current-voltage characyteristics. The contacts were prepared by indium soldering onto the freshly cleaved surfaces of the specimens which were in the form of a rectangular parallelepiped with 6 × 1.3 × 1.1 mm^3 dimensions (for $\mathbf{J} \| \mathbf{c} \perp \mathbf{H}$ geometry) and 5 × 1 × 1 mm^3 (for $\mathbf{J} \perp \mathbf{c} \| \mathbf{H}$ geometry). For the latter case the specimens were preliminary cut out and underwent subsequent grinding and polishing. Hall coefficient was measured at the magnetic field value of 8 KGs.

Figure 44 shows temperature dependences of $\sigma_{\|}$ and $\sigma_{\perp}$. Figure 45 shows the dependences of $R_{\|}$, $R_{\perp}$ and $\sigma_{\|}$, $\sigma_{\perp}$ on the pressure measured at room temperature. Hall coefficient $R_{\|}$ corresponds to the case when Hall field was measured situating the magnetic field along the **c**-axis and the current direction being perpendicular to it. $R_{\perp}$ corresponds to the case when the direction of the current and magnetic field are exchanged. The dependences given in Figures 44 and 45 are typical for n-TlSe crystals with the carrier concentration $n = 4 \times 10^{14}$ cm^{-3}. The authors of Ref.[130] analysed the experimental results assuming an intrinsic semiconductor since the value of TlSe bandgap known from the literature is close to the conductivity activation energy value (E_g) obtained from the experiment.

The conductivity activation energy obtained from $RT^{3/2}$ dependences (within 200–300 K) were similar for both cases ($R_{\|}$ and $R_{\perp}$) and equalled to 0.66 eV. As for the values of E_g determined from the temperature dependences of $\sigma_{\|}$ and $\sigma_{\perp}$, they appeared to be equal to $E_{g\|} = 0.66$ eV and $E_{g\perp} = 0.70$ eV, respectively. The error of determining E_g did not exceed ± 0.015 eV. The difference in conductivity activation energy values is equal to $E_g = E_{g\perp} - E_{g\|} = 40$ meV. Similar measurement carried out for the crystals from the other sets showed that the difference in conductivity activation energy values changed within 20–120 meV.

It is shown in Ref.[130] that four ellipsoids situated at the Brillouin band edge in the middle of symmetric line D are isoenergetic surfaces for electrons in TlSe. Rotation ellipsoid which is also situated at the Brillouin band edge in highly symmetrical point T, is a p-type surface. According to Ref.[131], Hall constant is anisotropic for the electrons. In the case of the isotropic relexation time [131]:

$$\frac{R^e_{\|}}{R^e_{\perp}} = \frac{4m^e_1/m^e_2}{(1 + m^e_1/m^e_2)^2} \,. \tag{30}$$

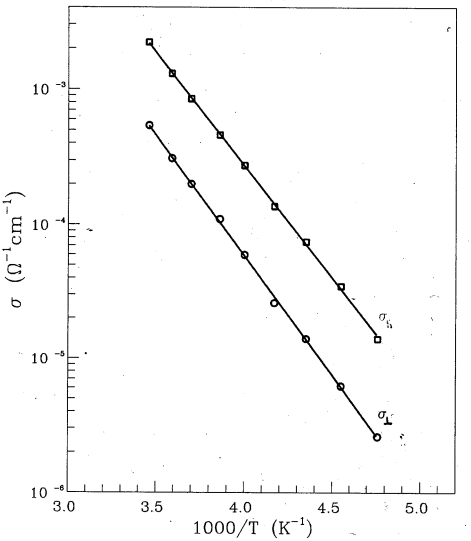


Figure 44. Temperature variation of the conductivity for TlSe with carrier concentration $4 \times 10^{14}\ cm^{-3}$ at room temperature and atmospheric pressure. The $\|$ and $\perp$ indices show the direction of current with respect to the tetragonal **c**-axis in the corresponding conductivity measurements

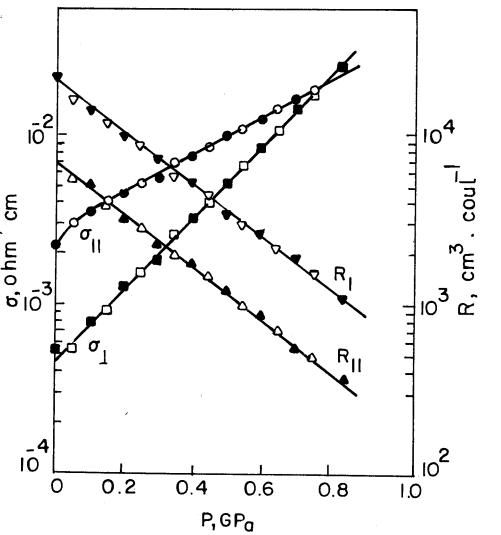


Figure 45. $\sigma_{\|}$ and $\sigma_{\perp}$ (the notations are the same as in Fig.44), $R_{\|}$ and $R_{\perp}$ (the magnetic field direction w.r.t. the **c**-axis) vs. pressure, taken at room temperature. Dark characters represent pressure increase and the light ones represent decrease

For the intrinsic TlSe semiconductor using the results of Ref.[131] one can write

$$\sigma_{\|} = ne\nu_{\|}(1 + b_{\|}) \tag{31}$$

$$\sigma_{\perp} = ne\nu_{\perp}(1 + b_{\perp}) \tag{32}$$

$$R_{\perp} = \frac{1}{ne}\frac{1 - b_{\|}b_{\perp}}{(1 + b_{\|})(1 + b_{\perp})} \tag{33}$$

$$R_{\|} = \frac{1}{ne}\frac{b_{\perp}^2(1 - b_1 b_2)}{b_1 b_2(1 + b_{\perp})^2}. \tag{34}$$

Here $b_i = \mu_i/\nu_i$; μ_i is the hole mobility; $\nu_{\perp} = \frac{1}{2}(\nu_1 + \nu_2), \nu_1, \nu_2, \nu_{\|}$ are partial mobilities of the same valley electrons. Indices $\|$ and $\perp$ show tetragonal crystal axis parallel and perpendicular directions, respectively. According to Eqns.(30–33), one should expect an anisotropy of electrical conductivity and Hall constant in thallium selenide crystals. But using these formulas for interpretation of the experimental data obtained in Ref.[130] one cannot explain observed anisotropy of the conductivity activation energy (ΔE_g = 40

meV). At the same time the experimental results can qualitatively be explained if the notions developed in Ref.[132] for the inhomogenous crystal conductivity are applied to thallium selenide.

Let us assume that TlSe consists of macroscopic cilindrical regions situated at random inside the crystal and extended along the **c**-axis with various conductivity activation energy and, consequently, with various concentrations of charge carriers. On such an assumption the conductivity along the tetragonal axis is equal to the total conductivity of separate regions and, as a result, the conductivity activation energy is determined by the least of activation energies

$$\sigma_{\parallel} \sim e^{-E_g^{min}/2k_oT} \tag{35}$$

The electrical conductivity in the crystal **c**-axis perpendicular direction will be equal to the reverse value of the total of separate region resistance; consequently, the largest activation energy region will make the basic contribution to $\sigma_{\perp}$,

$$\sigma_{\perp} \sim e^{-E_g^{max}/2k_oT}. \tag{36}$$

Thus, it is the difference in activation energies $\Delta E_g = E_g^{max} - E_g^{min}$ that determines the value of the potential barrier stimulated by the above-mentioned disorder. The possible cause of the latter will be considered hereafter.

On the disordered crystal assumption one can also explain the equality of activation energy values derived from the experimental $R_{\perp}T^{3/2}$ and $R_{\parallel}T^{3/2}$ dependences. In Ref.[132] it is shown that Hall coefficient value in disordered systems is determined by charge carrier concentration in the region with maximum concentration, i.e., with the lowest activation energy,

$$R_{\parallel,\alpha} \sim e^{-E_g^{min}/2k_oT}. \tag{37}$$

One can see from Fig.45 that with pressure increase the $\sigma_{\parallel}/\sigma_{\perp}$ ratio decreases and at $P = 7.6$ $kbar$ it is equal to 1. It is experimentally established that ΔE_g does not depend on temperature within 200–300 K and decreases under pressure at room temoerature. Baric coefficients of conductivity activation energy determined from $\sigma_{\parallel}$ and $\sigma_{\perp}$ dependences (Fig.45) are equal to $\partial E_{g\parallel}/\partial P = -1.3 \times 10^{-5}$ eV/bar and $\partial E_{g\perp}/\partial P = -2.4 \times 10^{-5}$ eV/bar, respectively. Thus, one succeeds in qualitative explanation of the baric features of kinetic effects in TlSe at standard conditions within the notions on the conductivity and Hall effect of a disordered crystral which consists of the regions with various conductivity activation energies. As the pressure increases the interaction between the regions increases too, this leading to their activation energy equalization and, hence, to the decrease of electrical conductivity anisotropy.

The deviation of selenium atoms from their equilibrium positions due to the totally symmetric A_{1g} type vibrations [133] can be the cause of the above mentioned disorder in TlSe. From the estimates given in Ref.[127], it follows that the uncertainty is $\Delta X = \pm 0.001$ in the value of the parameter X =0.179, which determines the position of selenium atoms in the crystal unit cell, is sufficient to explain experimentally observed difference $\Delta E_g = 40$ meV.

It should be noted that according to Refs.[134] and [135], the value of $\Delta X = \pm 0.001$ is within the error which determines the position of selenium atoms by X cordinate. Pressure increase leads to interaction increase between the chains, which in turn, can lead to the equilibrium positions of selenium atoms being averaged, i.e., the parameter X becomes approximately equal for the selenium atoms situated in two neighboring chains. The latter results in the decrease of disorder level and of the ratio of anisotropy parameters connected with this.

Anisotropy of the baric coefficients $\partial E_{g\perp}/\partial P > \partial E_{g\parallel}/\partial P$ can be explained by the following considerations. The crystal inhomogenity is due to the potential barrier Δ. Then one can write $\sigma_{\parallel} \sim e^{(-E_g(0)-\Delta)/2k_0T}, \sigma_{\perp} \sim e^{(-E_g(0)+\Delta)/2k_0T}$, where $E_g(0)$ is the value of conductivity activation energy of an ideal (not disordered) crystal. According to Eqns.(35) and (36), $E_g^{min} = E_g(0) - \Delta$ and $E_g^{max} = E_g(0) + \Delta$.

It is known that TlSe bandgap decreases under pressure [127]. Assuming that the barrier value also decreases with pressure increase it is easy to show that the existence of potential barrier Δ leads to the anisotropy of bandgap baric coefficients in TlSe crystals. At that if the average value is taken from experimentally determined ones $\partial E_g^{max}/\partial P$ and $\partial E_g^{min}/\partial P$, i.e., if one neglects the potential barrier in the crystal, the value of -1.85×10^{-5} eV/bar will be obtained. The value of baric coefficient of indirect bandgap calculated theoretically in Ref.[127] for an "ideal" TlSe crystal, without taking into account potential barriers is equal to $\partial E_g^i/\partial P = -2.1 \times 10^{-5}$ eV/bar.

It is necessary to calculate electron and hole mobilities for qualitative estimation of the anisotropy level of electrical conductivity and Hall effect in TlSe. Using the data given in Ref.[127] on the effective electron ($m_1^e = 0.84m_o$, $m_2^e = 0.75m_o$, $m_3^e = m_{\parallel}^e = 0.27m_o$) and hole ($m_{\perp}^h = 0.32m_o$, $m_{\parallel}^h = 4.4m_o$) masses as well as the values of deformation potentials [136] it is easy to show that the scattering at the low-frequency phonons is not determinant and makes a small contribution into the charge carrier mobilities.

Only the scattering at polar optical phonons with the frequency of $w_l = 177cm^{-1}$ and with an effective charge $e_s = 0.26e$ [133] reasonably (in comparison with experimental one) estimates by the order of magnitude the electron and hole mobility $\nu_{\perp} = 240$, $\nu_{\parallel} = 445$, and $\mu_{\perp} = 270$, $\mu_{\parallel} = 20$ $cm^2/Vsec$. Using these values in Eqns.(31–34) one can estimate the expected parameters of the anisotropy of electrical conductivity and Hall constant. We obtained at that $\sigma_{\parallel}/\sigma_{\perp} \sim 0.92$. One can see that the crystal conductivity is weakly dependent on the direction without taking into account the potential barrier.

Hall constants are $R_{\perp} \sim -0.42/ne$, $R_{\parallel} \sim 0.09/ne$, and their ratio is $R_{\parallel}/R_{\perp} \sim -0.21$. One can see that the estimated value is in reasonable agreement with one obtained from the experiment. Moreover, the calculation shows that for the case of $\mathbf{J} \perp \mathbf{c} \| \mathbf{H}$ in comparison with $\mathbf{J} \| \mathbf{c} \perp \mathbf{H}$ the change of the Hall constant sign should be expected, the latter being in full agreement with the experiment.

5. Conclusion

In this review there has been no attempt to provide a comprehensive overview of all existing publications devoted to the phase transitions in ternary layered chalcogenides in the literature. Indeed, with a rapidly increasing activities in this field over a broad range of topics, that would be a rather difficult task. We believe, however, that this review provides some initial and necessary results which show that ternary layered chalcogenide semiconductors could be considered as a comparatively novel class of semiconducting ferroelectrics and are interesting objects for phase transition investigations at comparatively high temperatures and moderate pressures.

Some of the works on weak ferroelectricity and on temperature dependences of longitudinal and transverse ultrasonic wave velocities in the directions parallel and perpendicular to the plane of layers were not included in this review. In the near future it would seem interesting to perform detailed low temperature (high pressure) x–ray and neutron diffraction measurements for identification of the crystal structures of $A^3B^3C_2^6$ materials at different phases, and to perform magnetoabsorption experiments in submillimeter region to find toroic-type vibrations, and to develope a model explaining the nature of ferroelectricity and negative regions of thermal expansion coefficients.

Acknowledgements The authors are greatful to Prof. Eldar Salaev and Prof. Hasan Abdullaev for their support and to Prof. Dr. Cengiz Yalçın for his encouragement for the preparation of this review. The authors would also like to thank to Dr. Zehra Salaeva for many technical assistance during the preparation of the manuscript.

References

[1] G. Abdullaev, K. Allakhverdiev, E. Vinogradov, G. Zhizhin, N. Melnik, E. Salaev and R. Sardarly, *Dokl. Akad. Nauk. Azerb. SSR*, **33** (1977) 26.

[2] E. Vinogradov, G. Zhizhin, N. Melnik, S. Subbotin, V. Panfilov, K. Allakhverdiev, E. Salaev and R. Nani, *Phys. Stat. Sol. b*, **95** (1979) 383.

[3] R. Aliev, K. Allakhverdiev, A. Baranov, N. Ivanov and R. Sardarly, *Sov. Phys. Solid State*, **26** (1984) 775.

[4] G.R. Offergeld, *Semiconducting materials containing thallium*, U.S.Patent **3**, 110 (1963) 685.

[5] G. Guseinov, A. Ramazanzade, E. Kerimova and M. Ismailov, *Phys. Stat. Sol.* **22** (1967) K112–K117.

[6] G. Guseinov, R. Gamidov, I.Kh. Mamedov, *Materiali Konferentsii Molodykh Uchenic, Inst. Neorg. Phys. Chim. Akad. Nauk Azerb. SSR*, **2**, (1968) 301.

[7] G. Guseinov, E. Mooser, E. Kerimova, R. Gamidov, I. Alakseev and M. Ismailov, *Phys. Stat. Sol* **34** (1969) 33.

[8] G. Guseinov, G. Abdullaev, S. Bidzinova, F. Seidov, M. Ismailov, A. Pashaev, *Phys. Rev. Lett.* **A33** (1970) 421.

[9] G. Guseinov, R. Gamidov, I.Kh. Mamedov, *Izvest. Akademii Nauk Azerb. SSR*, **25** (1969) 301.

[10] G. Guseinov, F. Seidov, Kh. Khalilov and M. Ismailov, *Zh. Phys. Chim.*, **46** (1972) 803.

[11] M. Babanly, A. Kuliev, *Izvest. Vyssh. Uchebn. Zaved. Khim. i Khim. Technol. SSSR*, **19** (1976) 1316.

[12] A. Kuliev and Z. Kagramanyan, *Izvest. Vyssh. Uchebn. Zaved. Khim. i Khim. Technol. SSSR*, **20** (1977) 606.

[13] M. Babanly and A. Kuliev, *Uchenie Zapiski Ministr. Vyssh. Sredn. Spets. Obraz. Azerb. SSR, Seria Chim Nauk.*, (1976) 31.

[14] A. Mamedov, *Dokl. Akad. Nauk. Azerb. SSR*, **34** (1978) 44.

[15] G. Guseinov, F. Seidov, A. Pashaev, Kh. Khaliliov and R. Nani, *Izvest. Akad. Nauk SSSR, Neorg.Mater.*, **8** (1972) 170.

[16] A. Bakhyshov, Z. Khalafov, A. Akhmedov, G. Guseinov and V. Tagirov, *Uchenie Zapiski Ministr. Vyssh. Sredn. Spets. Obraz. Azerb. SSR, Seria Fiz. Techn. i Mat. Nauk*, (1977) 58.

[17] A. Bakhyshov, A. Lebedev, Z. Khalafov and M.A. Yakobson, *Sov. Phys. Semicon.*, **12** (1978) 320.

[18] A. Bakhyshov, Z. Khalafov, A. Akhmedov, V. Salmanov and V.Tagirov, *Fiz. Techn. Poluprov.*, **10** (1976) 1950.

[19] I. Karpovich, A. Chervova, L. Demidova, E. Leonov and V. Orlov, *Izvest. Akad. Nauk SSSR. Seria Neorg. Mater.*, **8** (1972) 70.

[20] L. Karpovich, A. Chervova and L. Demidova, *Izvest. Akad. Nauk SSSR, Seria Neorg. Mater.*, **10** (1974) 2216.

[21] A. Bakhyshov, L. Gasanova and A. Lebedev, *Izvest. Akad. Nauk SSSR, Seria Neorg. Mater.*, **13** (1977) 366.

[22] L. Demidova, A. Chernova, L. Karaseva and M. Shilova, *Izvest. Vyssh. Ucheb. Zaved SSSR, Seria Fiz.*, **21** (1978) 134.

[23] A. Bakhyshov, A. Darvish and V. Tagirov, *Uchenie Zapiski Azerb. Univers. Ser. Fiz-Mat. Nauk.*, (1978) 126.

[24] T. Vischakas, T. Vaitkus, G. Guseinov, S. Abdullaeva, F. Seidov, M. Ismailov and Kh. Khalilov, *Material Research Bull.*, **11** (1976) 377.

[25] L. Musaeva, A. Mamedov, A. Bakhyshov, L. Kasumova and Sh. Efendiev, *Sov. Phys. Solid State*, **18** (1976) 822.

[26] L. Musaeva, Z. Khalafov, N.M. Gasanly and A. Bakhyshov, *Uchenie Zapiski Ministr. Vyssh. Sredn. Obraz. Azerb. SSR, Ser. Fiz. Tekh.-Mat. Nauk*, **N5** (1975) 88.

[27] T. Isaacs and R. Hopkins, *J. Cryst. Growth*, **29** (1975) 121.

[28] G. Guseinov, F. Seidov, Kh. Khalilov and M. Ismailov, *J. Phys. Chem USSR, Deponent*, (1971) 3761.

[29] A. Kuliev and M. Babanly, *Uchenie Zapiski Ministr. Vyssh. Sredn. Spets. Obraz. Azerb. SSR, Ser. Fiz. Tekh.-Mat. Nauk*, (1975) 27.

[30] L. Musaeva, A. Bakhysov, M.N. Gasanly, Z. Khalafov, *Rukopis Dep. VINITI*, (1975) 3762.

[31] A. Chervova, *Uch. Zap. Gork. Univ. Ser. Phys.*, **N126** (1971) 29.

[32] I.A. Karpovich, A. Chervova, E. Leonov and V. Orlov, *Phys.Stat.Sol.a*, **4** (1971) K13.

[33] A. Bakhysov, L. Musaeva, A. Lebedev and M. Yakobsen, *Sov. Phys. Semicon.*, **9** (1975) 1021.

[34] H. Hahn and B. Welmann, Naturwiss. **54** (1967) 42.

[35] T. Isaacs and J. Feichtner, *J. Solid. State Chem.*, **14** (1975) 260.

[36] D. Müller and H. Hahn, *Z. Anorg. Allg. Chem.*, **438** (1978) 258.

[37] K. Range, G. Mahlberg and S. Oberland, *Z. Naturforsch.*, **B32** (1977) 1354.

[38] V. Slivka, V. Gerasimenko, A. Zhdankin, Yu. Voroshilov, I. Nekrasova and M. Golovei, *Izvest. Vyssh. Uchebn. Zaved. SSSR, Ser. Fiz.*, **20** (1977) 158.

[39] A. Bolagurov, M. Dlounga and G. Mironova, *Report JINR (Dubna)*, (1978) R–14–11981.

[40] T. Kabre, *These Doctorat es Sciences*, Paris, Juin 1974.

[41] D. Müller, F. Poltman, H. Hahn, *Z. Naturforsch.* **29B** (1974) 117.

[42] T. Isaacs, *Z. Crystallogr.*, **147** (1975) 104.

[43] B. Mavrin, Kh. Sterin, N.M. Gasanly, Z. Khalafov, E. Salaev, K. Allakhverdiev and R. Sardarly, *Sov. Phys. Solid State*, **19** (1977) 1734.

[44] W. Henkel, H. Hochheimer, C. Carlone, A. Werner, S. Ves and H. Schnering, *Phys. Rev.*, **B26** (1982) 3211.

[45] N.M. Gasanly, B. Dzhavadov, A. Ragimov, V. Tagirov, R. Guseinov, *Physica*, **112B** (1982) 78.

[46] N.M. Gasanly, A. Goncharov, N. Melnik, A. Ragimov and V. Tagirov, *Phys. Stat. Sol. b*, **116** (1983) 427.

[47] K. Allakhverdiev, F. Wondre, J. Ryan and R. Sardarly, *Phys. Stat. Sol. b* **88** (1978) K5.

[48] G. Abdullaev, K. Allakhverdiev, E. Vinogradov, G. Wollf, G. Zhizhin, N. Melnik, E. Salaev and R. Sardarly, *Mater. Vsesoysnoi Konferentsii Spectroscopyji KRS, Moscow, Nauka* (1978).

[49] M. Agladze, B. Antonuk, B. Burlakov, E. Vinogradov and G. Zhizhin, *Sov. Phys. Solid State*, **23** (1981) 1911.

[50] A. Volkov, Yu. Goncharov, G. Kozlov, S. Lebedev, A. Prokhorov, R. Aliev and K. Allakhverdiev, *Pisma ZETF*, **37** (1983) 517.

[51] A. Volkov, Yu. Goncharov, G. Kozlov, K. Allakhverdiev and R. Serdarly, *Sov. Phys. Solid State*, **25** (1983) 2061.

[52] A. Volkov, Y. Ishibashi, G. Kozlov, S. Lebedev, J. Petzilt and A. Prokhorov, *J. Phys. Soc. Japan*, **49**, suppl. B78 (1980) 429.

[53] A. Volkov, Yu. Goncharov, G. Kozlov and R. Serdarly, *Pisma ZETF*, **39** (1984) 293.

[54] S. Abdullaeva, S. Abdinbekov and G. Guseinov, *Dokl. Akad. Nauk. Azerb. SSR*, **8** (1980) 34.

[55] V. Dvorak and J. Petzelt, *J. Phys. C: Solid State Phys.*, **11** (1978) 4827.

[56] Yu. Kopaev and V. Tugushev, *Pisma ZETF*, **41** (1985) 320.

[57] A. Gorbatsevich, Yu. Kopaev and V. Tugushev, *Pisma ZETF*, **85** (1983) 1107.

[58] V. Dubovik and Z. Tasuajian, *Pisma ZETF*, **14** (1983) 1193.

[59] A. Volkov, Yu. Goncharov, G. Kozlov, K. Allakhverdiev and R. Sardarly, *Sov. Phys. Solid State*, **26** (1984) 1668.

[60] S. Vakhrushev, V. Zhdanova, B. Kvyatkovskii, N. Okuneva, K. Allakhverdiev, R. Aliev and R. Serdarly, *Pisma ZETF*, **39** (1983) 245.

[61] N. Abdullaev, K. Allakhverdiev, G. Belenkii, T. Mamedov, R. Suleimanov and Ya. Sharifov, *Solid State Commun.*, **53** (1985) 601.

[62] N. Abdullaev, K. Allakhverdiev, G. Belenkii, T. Mamedov, R. Suleimanov and Ya. Sharifov, *Dokl. Acad. Nauk Azerb. SSR*, **16** (1985) 21.

[63] K. Allakhverdiev, S. Babaev, N. Bakhyshov, T. Mamedov, *Preprint IFAN Azerb. SSR*, **N122** (1985) 14.

[64] A. Bailey and B. Vates, *J. Appl. Phys.* **41** (1970) 5088.

[65] B. Vates, M. Overy and O. Pirgon, *Phil.Mag.* **32** (1975) B47.

[66] G. Belenkii, S. Abdullaeva, A. Solodukhin and R. Suleimanov, *Solid State Commun.* **44** (1982) 1613.

[67] G. Belenkii, R. Suleimanov, N. Abdullaev and V. Steinshraiber, *Sov. Phys. Solid State*, **26** (1984) 2142.

[68] S. Vakhrushev, B. Kujatkovski, N. Okuneva, K. Allakhverdiev and R. Sardarly, *Preprint Leningrad Fiz. Tekhn. Inst.* **N866** (1984) 12.

[69] D. Sannikov and V. Golovko, *Sov. Phys. Solid State*, **26** (1984) 678.

[70] K. Allakhverdiev, S. Guseinov, T. Mamedov and V. Steinshraiber, *Doklad. Akad. Nauk. Azerb. SSR*, **25** (1988) 153.

[71] K. Allakhverdiev, S. Babaev, M. Tagyev and M. Shirinov, *Phys. Stat. Sol. b* **152** (1989) 317.

[72] K. Allakhverdiev, N. Akhmed-zade, M. Tagyev, M. Shirinov and S. Haisaler, *Phys. Stat. Sol. b* **148** (1988) K93.

[73] R. Zallen, *Phys. Rev.* **B9** (1974) 4485.

[74] R. Loudon, *Adv. Phys.* **13** (1964) 423.

[75] B. Kulbujaev, Z. Rabkin, V. Tograshev and Yu.Izuk, *Fiz. Tverd. Tela*, **30** (1988) 195.

[76] K. Range, G. Engert, W. Miller and A. Weiss, *Z. Naturforsch.* **B29** (1974) 181.

[77] K. Allakhverdiev, R. Guliev, L. Kulevskii, A. Savelev, E. Salaev and V. Smirnov, *Phys. Stat. Sol. a*, **60** (1980) 309.

[78] A. Levanyuk, *Sov. Phys. JETP*, **22** (1966) 901.

[79] W. Rehvald and A. Vonlanten, *Solid State Commun.* **38** (1981) 209.

[80] E. Karajomaki, R, Laiho and T. Iuleva, *J. Phys. C: Solid State Phys.* **16** (1983) 1531.

[81] A.D. Prins, K. Allakhverdiev, S.S. Babaev, S.S. Guseinov, E.I. Mekhtiev, M.M. Shirinov, M.M. Tagyev and D.I. Dunston, *Phys. Stat. Sol. b*, **151** (1989) 759.

[82] B. Weinstein and R. Zallen, *Light Scattering in Solids IV: Electronic Scattering, Spin Effects, SERS and Morphic Effects*, Ed. by M. Cardona and Y. Guntherodt, Chapter 8, (Springer–Verlag, Heidelberg, 1984) p463.

[83] Y. Martinez, *Optical Properties of Semiconductors under Pressure*, Ed. M. Balkanski, Chapter 4c, (1980) p181, Vol.**2** of "Handbook on Semiconductors", Ed. by T.S. Moss.

[84] R. Zallen, *Scientific Report N10* (1974) 55.

[85] V. Panfilov, S. Subbotin, L. Vereschagin, I. Ivanov and L. Molchanova , *Phys. Stat. Sol. b* **72** (1975) 823.

[86] A. Nilisc and T. Kirs, *Phys. Stat. Sol. b* **31** (1969) K91.

[87] J. Besson, R. Toullec, J. Pinceaux, A. Chevy and H. Fair, *High-Temper.-High Pressure*, **7** (1975) 710.

[88] S. Subbotin, V. Panfilov, L. Vereschegin, L. Molchanova and G. Akhundov, *Dokl. Akad. Nauk. SSSR*, **202** (1972) 1039.

[89] S. Subbotin, V. Panfilov and L. Molchanova, *Phys. Stat. Sol. a*, **39** (1977) 357.

[90] A. Mejatty, A. Segura, R. Toullec, J. Besson, A. Chevy and H. Fair, *J. Phys. Chem. Sol.* **39** (1978) 25.

[91] J. Besson, *Il Nuovo Cimento* **38B** (1977) 478.

[92] M. Hayek, O. Brafman and R. Lieth, *Phys. Rev.***B8** (1973) 2772.

[93] E. Vinogradov, G. Zhizhin, N. Melnik, S. Subbotin, V. Panfilov, K. Allakhverdiev, S. Babaev and V. Zhitar, *Phys. Stat. Sol. b*, **99** (1980) 215.

[94] K. Allakhverdiev, E. Salaev, M. Tagyev, S. Babaev and L. Genzel, *Solid State Commun.* **59** (1986) 133.

[95] K. Allakhverdiev, T. Mamedov and M. Tagyev, *Physica i Tekhnika Visokish Davlenij*, **12** (1988) 55.

[96] T. Wieting, *Solid State Commun.* **12** (1973) 931.

[97] K. Allakhverdiev, S. Babaev, E. Salaev, M. Tagyev, E. Vihogradov, A. Goncharov, N. Melnik, S. Subbotin and V. Panfilov, *Solid State Commun.* **35** (1980) 705.

[98] L.K. Vodofyanov, L. Golubev and K. Allakhverdiev, *Sov. Phys. Solid State*, **21** (1979) 1431.

[99] F. Cerdeira, E. Meneses and A. Gouskov, *Phys. Rev.* **B16** (1977) 1648.

[100] J. Irwin, B. Clayman and D. Mead, *Phys. Rev.* **B19** (1979) 2039.

[101] K. Allakhverdiev, N. Safarov, M. Nizametdinova, E. Vinogradov, N. Melnik, A. Goncharov and S. Subbotin, *Solid State Commun.* **42** (1982)485.

[102] K. Allakhverdiev, M. Nizametdinova, R. Nani, E. Salaev, R. Sardarly, N. Safarov, E. Vinogradov, G. Zhizhin and L. Golabev, *Preprint IFAN Azerb. SSR*, **N8** (1978) 32.

[103] K. Allakhverdiev, E. Salaev, N. Safarov, L. Vodopyanov and L. Golubev, *Phys. Stat. Sol. b* **92** (1979) K91.

[104] M. Nizammetdinova, D. Guseinov and V. Steinshraiber, *Sov. Phys. Solid State*, **19** (1977) 1177.

[105] K. Allakhverdiev, T. Mamedov, G. Peresoda, E. Ponijatovskij and J. Sharifov, *Sov. Phys. Solid State*, **27** (1985) 568.

[106] K. Allakhverdiev, T. Mamedov and M. Shukurov, *Preprint IFAN Azerb. SSR,* **N142** (1985) 33.

[107] K. Allakhverdiev, T. Mamedov, V. Panfilov, S. Subbotin and M. Shukyrov, *Fiz. Tekhn. Poluprov*, **20** (1986) 342.

[108] H. Amour, W. Holzapfel, A. Polian and A. Chevy, *Solid State Commun.* **44** (1982) 853.

[109] K. Allakhverdiev, T. Mamedov, S. Subbotin and M. Shukyrov, *Sov. Phys. Solid State*, **28** (1986) 1012.

[110] F. Urbach, *Phys. Rev.* **92** (1953) 1324.

[111] V. Zametin, M. Jacubovski and L. Rabkin, *Sov. Phys. Solid State*, **21** (1979) 291.

[112] T. Mamedov, V. Panfilov, S. Subbotin, M. Shukyrov and I. Efendieva, *Abstracts of all Union Conf. on Phys. of Semicon., Baku, October 12–15*, (1982) 242.

[113] K. Allakhverdiev, S. Babaev, N. Bakhyshov, T. Mamedov, G. Peresada, M. Shukyrov and E. Salaev, *Sov. Phys. Semicon.* **18** (1984) 817.

[114] K. Allakhverdiev, T. Mamedov, V. Panfilov, M. Shukyrov and S. Subbotin, *Phys. Stat. Sol. b*, **131** (1985) K23.

[115] A. Levikin and V. Vavakin, "Methods of measurements of the elastic properties of solids" in *Physical Properties of Materials under High Pressure, Moscow* (1978) 18.

[116] K. Allakhverdiev, A. Baranov, T. Mamedov, V. Sandler and Ya. Sharifov, *Ferroelectrics Letter Sect.* **8** (1988) 323.

[117] A. Shirokov, A. Baranov and L. Shuvalov, *Izvest. Akad. Nauk. SSSR Ser. Fiz.* **35** (1971) 1903.

[118] K. Mamedov, A. Abdullaev and E. Kerimova, *Phys. Stat. Sol. a* **94** (1986) 115.

[119] E. Krupnikov, F. Aliev and V. Aliev, *Preprint IFAN Azerb. SSR,* **N280** (1988) 29.

[120] A. Beligaev, Yu. Golobobov, K. Allakhverdiev, T. Mamedov and Ya. Sharifov, *Abstracts of all Union Conf. on Phys. of Ferroelectricity* **2** (1986) 45.

[121] G. Abdullaev, G. Abytalibov, A. Aliev, L. Larionkina, I. Neriman-zade and E. Salaev, *Pisma ZETF*, **38** (1983) 525.

[122] A. Krasnikova, I. Polandov, V. Milov, *Sov. Phys. Solid State*, **8** (1966) 1967.

[123] V. Vaks, *Introduction to the Microscopic Theory of Ferroelectricity, Moscow, Nauka* (1973) 327.

[124] K. Allakhverdiev, Sh. Gasymov, T. Mamedov, E. Salaev and I. Efendieva, *Phys. Stat. Sol. b*, **113** (1982) K127.

[125] K. Allakhverdiev, S. Babaev, N. Bakhyshov, T. Mamedov, E. Salaev and I. Efendieva, *Phys. Stat. Sol. b*, **126** (1984) K139.

[126] K. Allakhverdiev, N. Bakhyshov, S. Guseinov, T. Mamedov, M. Nizametdinova and I. Efendieva, *Phys. Stat. Sol. b*, **147** (1988) K99.

[127] F. Gashimzade and G. Orudjev, *Sov. Phys. Semicon.* **15** (1981) 757.

[128] K. Allakhverdiev, T. Mamedov, E. Salaev and I. Efendieva, *Phys. Stat. Sol. b*, **13** K43.

[129] K. Allakhverdiev, T. Mamedov, V. Steinshraiber and I. Efendieva, *Phys. Stat. Sol. b*, **127** (1985) K55.

[130] K. Allakhverdiev, Sh. Gasymov, T. Mamedov, M. Nizametdinova and E. Salaev, *Sov. Phys. Semicon.* **17** (1983) 131.

[131] F. Gashimzade, *Izvest. Akad. Nauk. Azerb. SSR*, **6** (1962) 83.

[132] A. Shik, "Conductivity in Anisotropic Sytems", *Proc. of 7th Winter School on the Physics of Semiconductors, Leningrad Ins. for Nuclear Physics, AN SSSR, Leningrad* (1975).

[133] K. Allakhverdiev, M. Nizametdinova, E. Salaev, R. Serdarly, N. Safarov, E. Vinogradov and G. Zhizhin, *Solid State Commun.* **36** (1980) 527.

[134] J. Ketelear, W. Mart, M. Moereland D. Polder, *Z. Kristallogr.* **101A** (1939) 396.

[135] R. Wyskoff, *Crystal Structure, Intern. Publ., NY* (1965) 280.

[136] R. Laiho, T. Levola, R. Sardarly, K. Allakhverdiev, I. Sadikov and M. Tagyev, *Solid State Commun.* **3** (1988) 315.

View publication stats